Article | Received 5 March 2025; Accepted 3 June 2025; Published 7 July 2025
https://doi.org/10.55092/cle20250001

Geochronology and geochemistry of mafic rocks in the Wutai area, North China: constraints on the latest Neoarchean–Paleoproterozoic tectonic setting of the Trans-North China Orogen and the onset of plate tectonics

Zubair Raja Asim, Jingyu Wang, Bin Wu, Caiyun Lan and Xiaoping Long*

State Key Laboratory of Continental Evolution and Early Life, Department of Geology, Northwest University, Xi'an 710069, China

* Correspondence author; Email: longxp@nwu.edu.cn.

Highlights:

- The ~2.54 Ga gabbros in the Wutai Complex originated from a juvenile, depleted mantle wedge metasomatized by slab-derived melts.
- The ~2.08 Ga amphibolites in the Wutai Complex were generated partial melting of garnet-spinel lherzolite and spinel lherzolite mantle sources metasomatism by slab-derived fluids and sediment melts.
- A tectonic transition from Late Archean oceanic subduction to Paleoproterozoic lithospheric extension occurred in the North China Craton.
- Plate tectonics at least partly happened most likely in the latest Neoarchean.

Abstract: The Neoarchean-Paleoproterozoic is a key period for the North China Craton due to the formation of continental crust and the beginning of oceanic subduction. The amalgamation of the Eastern and Western blocks of the North China Craton remains debated, particularly regarding the timing, directionality (eastward *vs.* westward subduction), and number of collisional phases. Previous studies disproportionately focus on felsic lithologies, creating a critical mafic blind spot that obscures insights into mantle dynamics and crust-mantle interactions. Systematic investigation of Late Archean to Paleoproterozoic mafic suites was essential to reconcile conflicting tectonic models and refine the craton's amalgamation history. In order to constrain the complex geological processes more clearly, we present new whole-rock geochemistry and zircon U-Pb geochronology for mafic rocks in the Wutai Complex. The Late Archean (2.56~2.54 Ga) gabbros are characterized by relatively depleted Nb–Ta and Zr–Hf anomalies, slightly positive Eu* anomalies, low K_2O concentrations, enrichments of LILE (Ba, CS, Th, and Rb), differentiated HFSE patterns and moderate $Mg^{\#}$ values (43–53). They show positive $\varepsilon_{Nd}(t)$ values (+4.9–+6.1) and high $(^{87}Sr/^{86}Sr)_i$ ratios (0.70063–0.70091). Additionally, these gabbros have high Nb concentration (13.3–23.3) and display enrichments in light rare earth elements (LREE) $(La/Yb)_N = 7.00–8.96$), high-field strength elements (HFSE, e.g., Nb, Ta, Zr), and high Nb/U and Nb/La ratios, suggesting a derivation from an arc-like mantle source. The gabbro melts were generated by a

low degree of 4%–5% partial melting of garnet-spinel lherzolite mantle. The Paleoproterozoic (2.16~2.08 Ga) amphibolites also display depleted Nb-Ta and Zr-Hf anomalies, enriched light rare earth elements (LREEs), but show lower Eu* anomalies, $\varepsilon_{Nd}(t)$ values (+0.9–+1.2), and $(^{87}Sr/^{86}Sr)_i$ ratios (0.69770–0.69930). The amphibolites exhibit a geochemical signature marked by LREE enrichment, negative HFSE anomalies, and distinct Sm-Nd isotopic composition, suggesting a subduction-related magma source. The enrichment of Cs, Rb, Ba, and the depletion of Nb, Ta, P, and Ti, imply that their magma source was significantly modified by subducted crustal materials. The trace element ratios, such as K/Rb, Rb/Y, Nb/Y, Th/Zr, and so on, further indicate that the gabbros were derived from a mantle substantially altered by siliceous slab-derived melts, whereas the amphibolites originated from a mantle influenced by slab-derived melts and fluids. The amphibolites were generated by the 15% partial melting of garnet-spinel lherzolite and the 15% melting of spinel lherzolite at a shallower mantle source. In combination with the previously published data of mafic rocks in the Wutai Complex, we infer that the Late Archean gabbros suggest their derivation in a subduction-related setting, whereas the Paleoproterozoic amphibolites formed in a back-arc basin setting. These findings underscore a tectonic transition from Late Archean oceanic subduction to Paleoproterozoic lithospheric extension in the North China Craton, indicating that plate tectonics at least partly happened most likely in the latest Neoarchean.

Keywords: subduction zone; mantle wedge; metasomatism; the Wutai Complex; North China Craton

1. Introduction

The North China Craton, Tarim Craton, and South China Craton are the three main Archean blocks that jointly make up the Chinese continental assemblage. These blocks are encircled by Phanerozoic tectonic belts (Figure 1a) [1,2]. The North China Craton (NCC), that covers about 150,000 km² in dimensions, is primarily comprised of Mesoproterozoic to Triassic sedimentary sequences and middle to Late-Archean and Paleoproterozoic basement rocks [3,4]. The Wutai, Fuping, and Hengshan complexes, referred as the basement rocks, are located along the Shanxi-Hebei provincial border in northern China, within the Trans North China Craton. The complexes are prominent Neoarchean-Paleoproterozoic metamorphic terranes, which have attracted considerable attention from geologists both within China and internationally (Figure 1b) [5]. The Trans-North China Orogen (TNCO), which includes the Wutai Complex, is a major Late Paleoproterozoic collisional belt that combines Eastern and Western blocks [6–10].

Nevertheless, there is still disagreement regarding the tectonic processes and timing that led to the two blocks combining. According to certain research, the oceanic lithosphere between the two blocks was subducted eastward, which caused the convergence and, at around ~1.85 Ga, the final collision [11–15]. In contrast, some research suggests a subduction regime that is westward directed, with the final collision taking place at approximately 2.5 Ga [16–20]. A third model suggests a westward-directed subduction, followed by two distinct collisional events occurring at ~2.1 Ga and 1.9–1.8 Ga [21–25]. A Neoarchaean–Palaeoproterozoic arc-dominated juvenile crust with accreted tectonic elements (mélanges, oceanic remnants), high-pressure assemblages (granulites, retrograded eclogites), and a minor reworked basement is preserved by the Trans-North China Orogen (TNCO). Its structure includes linear fold belts with sheath folds and crustal-scale ductile shear zones, which record cycles of subduction, collision, and exhumation [26–30].

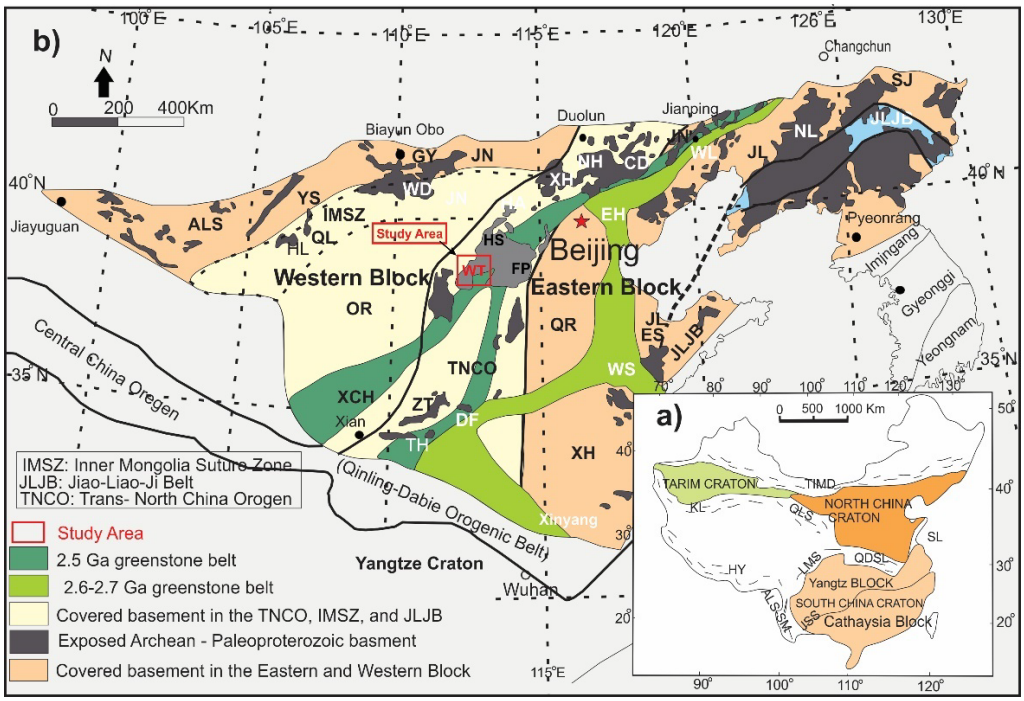

Figure 1. Tectonic subdivision of the North China Craton. **(a)** Precambrian blocks and Late Neoproterozoic and Paleozoic fold belts of China (Modified after [1,2]); **(b)** Tectonic framework of North China Craton, showing the basement rock, major macroblocks, and granite-greenstone belts. The Wutai Complex in central part of TNCO is marked in a red box and shown in Figure 1b (Modified after [28,29]). (Abbreviations in Figure 1a,b: HY, Himalaya fold belt; KL, Kunlun fold belt; QDSL, Qinling-Dabie-Su-Lu fold belt; QLS, Qilianshan fold belt; TIMD, Tianshan-Inner Mongolia-Daxinganling fold belt. Abbreviations of the microblocks in Figure 1b: ALS, Alashan block; OR, Ordos block; JN, Jining block; QH, Qianhuai block; XCH, Xuchang block; XH, Xuhuai block; JL, Jiaoliao block. Abbreviations of the metamorphic complexes in Figure 1b: CD, Chengde; EH, Eastern Hebei; ES, Eastern Shandong; FP, Fuping; GY, Guyang; HA, Huai'an; HL, Helanshan; HS, Hengshan; JN, Jining; LL, Lüliang; MY, Miyun; NH, Northern Hebei; NL, Northern Liaoning; QL, Qilianshan; SJ, Southern Jilin; SL, Southern Liaoning; TH, Taihua; WD, Wulashan-Daqingshan; WT, Wutai; WS, Western Shandong; XH, Xuanhua; YS, Yingshan; ZT, Zhongtiao; ZH, Zanhuang.)

Attempts to reconstruct the Wutai Complex's geological and tectonic history have been made numerous times [31–35]. In recent decades, there has been a lot of interest in the geochemical characteristics of mafic rocks in an attempt to understand their origins and the associated geodynamic processes [36–40]. These studies sought to distinguish between tectonic environments and learn more about the formation of igneous rocks and the geodynamic processes that underlie them [41–43]. TTG gneisses, calc-alkaline granitoids from the Wutai, Fuping, and Hengshan complexes, and the geochemical characteristics and Nd and Pb isotopic compositions of the Neoarchean to Paleoproterozoic [44], proposed a multicollisional model of the Trans North China Orogen (TNCO). Reference [45] categorized the Wutai Complex's mafic, intermediate, and felsic volcanic rocks and greenschist to amphibolite facies based on their geochemical properties and also proposed that the Wutai greenstone assemblage contains an association of the basalt-adakite and MORB-Arc types. Reference [18] acquired geochronological,

geochemical, and structural data pertaining to the Wutai terrane, indicating a forearc tectonic environment. However, these studies mostly concentrate on establishing the Wutai terrane's geodynamic context, largely ignoring the petrogenesis of mafic intrusions. The geodynamic processes and interactions between the Neoarchean crust and mantle must be understood in order to fully appreciate the petrogenesis of the Wutai mafic intrusions. Understanding the interactions between the subduction zones and the mantle wedge requires an understanding of subduction-related mafic intrusions. The metasomatism of melts or fluids produced by the subducted slab enriches the mantle wedge with large ion lithophile elements [46–50]. In the vicinity of a subduction zone, the mantle may encounter fluids and melts at varying depths [51–53]. Mafic rocks derived from the mantle in subduction zones may show varying degrees of alteration to their mantle sources due to the influence of slab-derived components [54]. Mafic rocks provide significant insights into the geodynamics associated with subduction environments. In this contribution, we present one Latest Neoarchean (2.54 Ga) and one Late Paleoproterozoic (2.08 Ga) zircon U–Pb ages for two mafic intrusions of the Wutai Complex, as well as new whole-rock geochemistry and Sm-Nd isotopic compositions, to explore the petrogenesis and geodynamics. Our results also provide insight into the Neoarchean and Late Paleoproterozoic tectonic settings, which give new evidence for the onset of plate tectonics and the Neoarchean to Late Paleoproterozoic tectonic evolution of the TNCO.

2. Geological settings

Archean to Paleoproterozoic rock assemblages, such as granitoids, orthogenesis, paragneisses, a range of extrusive volcanics from ultramafic to felsic, banded iron formations, and small units of carbonate and siliciclastic sedimentary rocks make up the North China Craton [5,55–57]. The Fuping Complex, characterized by medium to high-grade metamorphism, is situated at the southeastern edge of the Fuping-Wutai-Hengshan tectonic belt and the high grade metamorphic Hengshan Complex is located in the northwest. The Wutai Complex is located in the middle of these complexes. Since the last century, this area has drawn researchers due to its complex tectonics, significant rock exposure, variety of rock types, abundant mineral resources, and low to high-grade metamorphic rocks. The geochemical characteristics of meta-mafic rocks have been widely utilized in Precambrian research to investigate crustal evolution and geodynamic processes [58–63]. To examine the processes associated with plume-lithosphere interaction geochemical statistics and the isotopic composition data have been employed [64–66]. Isochron dating, geochemical and isotopic data of various meta-mafic rock units from the central belt of the North China Craton extensively documented [26,67–71]. The evolutionary history of the Trans North China Orogen (TNCO) and the importance of magmatic events from the Neoarchean to Paleoproterozoic have been clarified through the analysis of Nd isotopic compositions in granitoids and mafic rocks of the Fuping Complex. The Neoarchean Wutai Group is located in the northern part of the Wutai region (Figure 2).

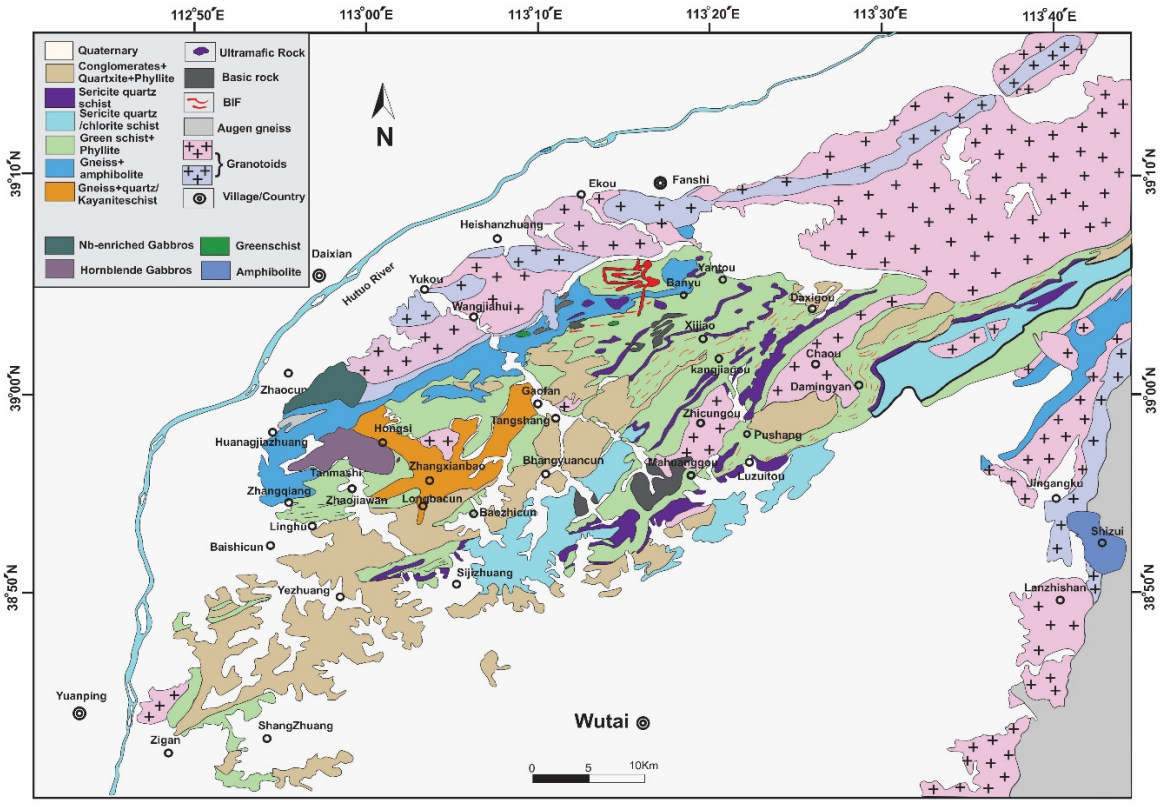

Figure 2. A simplified geological map of the Wutai area shows the sample collection location and rock type in red triangles and Black filled rectangles (modified after [8]).

The SHRIMP zircon dating of the Wutai Complex reveals that a significant portion of the granitoids intruded between 2566 and 2517 Ma, signifying the onset of juvenile crustal growth in the region [72,73]. The volcanic and sedimentary rocks of the Wutai Complex encompass a metamorphic spectrum from sub-greenschist to amphibolite facies. Field investigations and dating outcomes indicate that these metamorphic facies are juxtaposed [13,31]. On the basis of rock types, geochemical characteristics, metamorphic intensity, and geodynamic setting, the Wutai greenstone belt can be classified into four units (Figure 3). The sub-greenschist-facies turbidites include the Wutai greenschist-facies assemblage (WT), the Northern Jingangku amphibolite-facies assemblage (N-JGK), and the Southern Jingangku amphibolite-facies assemblage (S-JGK) [45]. Zircon SHRIMP dating indicates that the Wutai Complex formed between 2530 and 2515 Ma, based on the analysis of intermediate and felsic volcanic rocks [31].

The Late Neoarchean to Paleoproterozoic mafic intrusions in the Wutai Complex consist of gabbros and amphibolites. Gabbro and amphibolite samples were collected from newly identified sites in the Wutai area. Gabbros display a medium to coarse-grained texture and are primarily comprised of pyroxene, plagioclase, and feldspar. Sixteen gabbro samples (19WT-01 to 19WT-16) were obtained from Zhouchun Village, while thirteen amphibolite samples (19WT-71 to 19WT-84) were sourced from Shizui Village. The coarse-grained amphibolites primarily comprise amphibole, hornblende, and plagioclase. A summary of the rock type, geographic location, and mineral constituents of the sample is provided in (Table 1, Figure 4a–d).

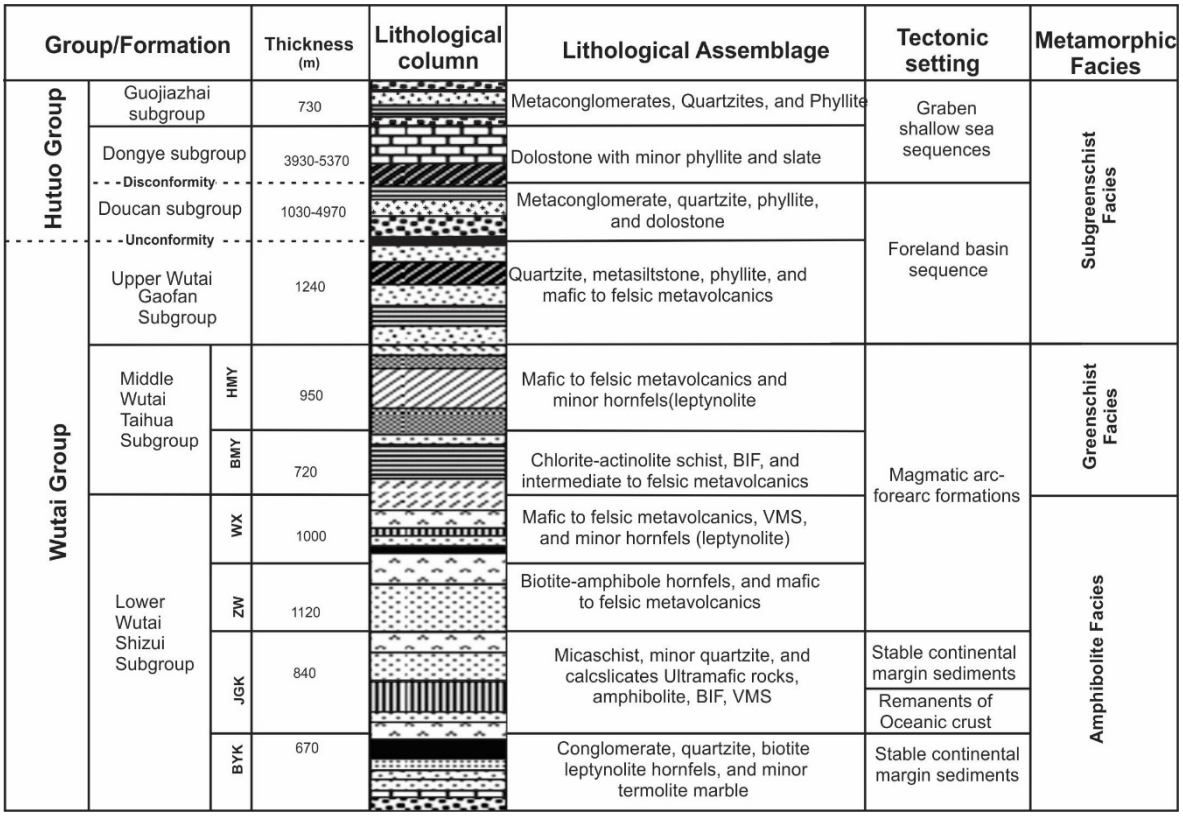

Figure 3. Stratigraphy, rock assemblage, and tectonic setting of the Wutai Complex (Modified after [71]). (Abbreviations for the formation names: BYK, Banyukou Formation; JGK, Jingangku Formation; ZW, Zhuangwang Formation; WX, Wenxi Formation; BZY, Baizhiyan Formation; HMY, Hongmenyan Formation.)

Figure 4. Representative field photographs of **(a)** Gabbro (19-WT-06) and **(b)** Gabbro (19WT-12), **(c)** Amphibolite (19-WT-71) and **(d)** Amphibolite (19-WT-83).

Table 1. Sample localities, rock types, GPS readings, and mineral assemblages of the Mafic Rocks from the Wutai Complex.

Sr.no	Samples	Rock Type	Location	GPS Coordinates	Mineral Assemblages
1	19WT-(01-10)	Gabbro	Zhoachun	N = 38° 59' 53", E = 112° 58' 24"	Cpx, Plg, Bt and Feo
2	19WT-(11-16)			N = 38° 59' 33", E = 112° 58' 39"	
3	19WT-(71-78)	Amphibolites	Shizui	N = 38° 53' 3", E = 113° 41' 0"	Amp, Hbl, Plg
4	19WT-(79-84)			N = 38° 52' 53", E = 113° 41' 17"	

3. Petrography of the gabbros and amphibolites

Petrographic analysis reveals that clinopyroxene, plagioclase, biotite and iron oxide dominate the composition of the fine-medium-grained gabbros (Figure 5a,b). Plagioclase makes up 40%–60% of the volume of the rock and is found as subhedral to anhedral crystals up to 0.2 mm. These crystals often have common sieve-textured core features and both normal and oscillatory zoning. Clinopyroxene, which makes up 20%–30% of the modal composition, is characterized by coarse grains that are about 0.4 mm in size and are frequently encircled by magmatic hornblende, which can make up as much as 10% of the rock. Five to ten percent of the rock is made up of iron-titanium oxides, which are sporadically distributed along grain boundaries and typically smaller than 0.2 mm. In contrast, the two main constituents of coarse-grained amphibolites are plagioclase and hornblende (Figure 5c,d). Hornblende constitutes 50%–70% modal composition, exhibiting prismatic, predominantly anhedral grains. Some grains may appear rounded, enclosed, or slightly altered by chlorite, suggesting low-temperature metamorphism. Plagioclase with an average grain size of 0.3 mm and the subhedral to anhedral crystals constitutes 30%–50% volume of the rock.

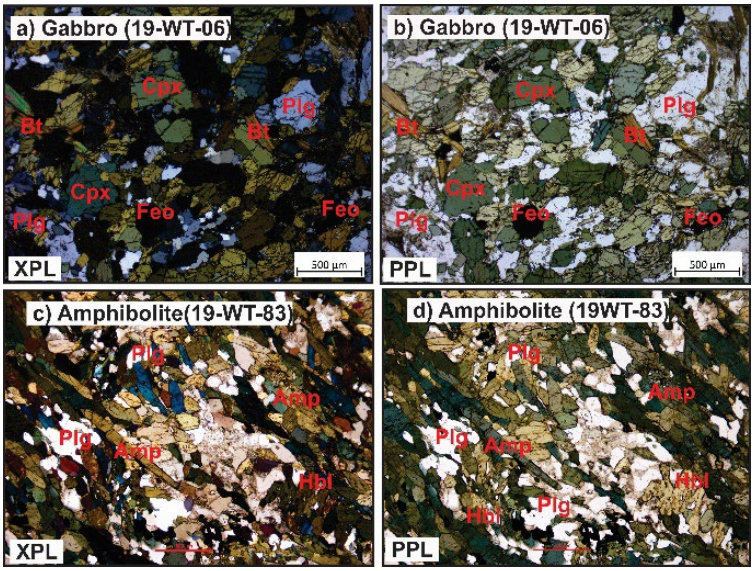

Figure 5. Photomicrographs of the **(a)** Gabbro in cross-polarized light (XPL), **(b)** Gabbros in plane-polarized light (PPL), composed of Clinopyroxene (Cpx), Plagioclase (Pl), Biotite (Bt), and Iron oxide (Feo), **(c)** Amphibolites in cross-polarized light (XPL), **(d)** Amphibolites in plane-polarized light (PPL), composed of Plagioclase (Pl), Amphibole, and Hornblende (Hbl). The scale bar is 500 µm.

4. Analytical methods

Geochronological analyses of zircon U-Pb and LA-ICP-MS trace element characterisation were performed at Guangzhou Tuoyan Analytical Technology Co., Ltd. in Guangzhou, China. Zircon underwent Sm-Nd isotopic analyses at the Guangzhou Institute of Geochemistry, State Key Laboratory of Isotope Geochemistry, and Chinese Academy of Sciences. Whole rock geochemical analyses were conducted by Guangzhou Tongwei Analytical Technology Co., Ltd. and Guangzhou Tuoyan Testing Technology Co., Ltd. The thorough descriptions of the methodologies employed in these analyses are provided in the Appendix, along with the analytical results.

5. Analytical results

5.1. Zircon U-Pb dating

Two samples from the mafic intrusions of the Wutai Complex were analysed using LA-ICP-MS zircon U-Pb dating, (19 WT-12) from gabbros and the (19 WT-71) from amphibolites (Figure 6a–d). The results of U-Pb dating and zircon rare earth geochemistry are described in the Supplementary Table 1. For gabbro sample 19 WT-12, twelve zircon spots yielded an average age of 2543 ± 20 Ma, with an upper intercept age of 2564 ± 35 Ma (Figure 6a,b). A cathodoluminescence (CL) image of zircon grains (Figure 7a) extracted from a gabbro sample (19WT-12), with U-Pb age dating results and Th/U ratios indicated for each analyzed grain. The zircon grains exhibit well-preserved internal zoning patterns, which are characteristic of igneous zircon crystallization. The U-Pb ages range from approximately 2414 Ma to 2574 Ma, indicating a Late Archean to Paleoproterozoic magmatic event. The majority of the zircon grains yield ages between 2500 Ma and 2570 Ma, suggesting a predominant crystallization period, while the younger age (2414 Ma) reflects later metamorphic or hydrothermal overprinting. The Th/U ratios of the analyzed zircons range from 0.4 to 1.1, with most values above 0.5, which is typically indicative of magmatic origin. The relatively higher Th/U values (e.g., 1.1) suggest a less evolved, mantle-derived melt, whereas lower Th/U values (~0.4) could indicate some degree of recrystallization or metamorphic influence. The consistency of high Th/U ratios in most grains supports the interpretation that the zircons primarily crystallized from a mafic magma rather than being inherited from older crustal sources.

The spread of U-Pb ages suggests that the gabbroic intrusion was emplaced during a Late Archean magmatic event, which is consistent with the broader tectonic evolution of the Wutai Complex within the North China Craton. The minor age variation and the presence of younger grains may imply post-magmatic thermal events or Pb-loss processes. These results contribute to the understanding of the petrogenesis and geodynamic significance of the Late Archean mafic magmatism in the region, potentially linking it to subduction-related processes or lithospheric reworking events.

In the amphibolite sample 19 WT-71, seven analyses provided an average mean age of 2087 ± 33 Ma and an upper intercept age of 2161 ± 58 Ma (Figure 6c,d). The zircons exhibit lengths ranging from 100 to 300 μm and length-width ratios ranging from 1:1 to 2:5 (Figure 7a,b). The cathodoluminescence (CL) image (Figure 7b) of zircon grains extracted from an amphibolite sample (19WT-71), with corresponding U-Pb ages and Th/U ratios indicated for each analyzed grain. The zircon grains exhibit well-developed internal zoning patterns, which are typical of igneous zircon crystallization but also reflect metamorphic overprinting. The U-Pb ages range from 1998 Ma to 2176 Ma, indicating a

Paleoproterozoic event. The majority of the ages fall between 2070 Ma and 2170 Ma (Figure 7b), suggesting a predominant period of zircon crystallization, while the younger grain at 1998 Ma indicates later metamorphic resetting or Pb loss.

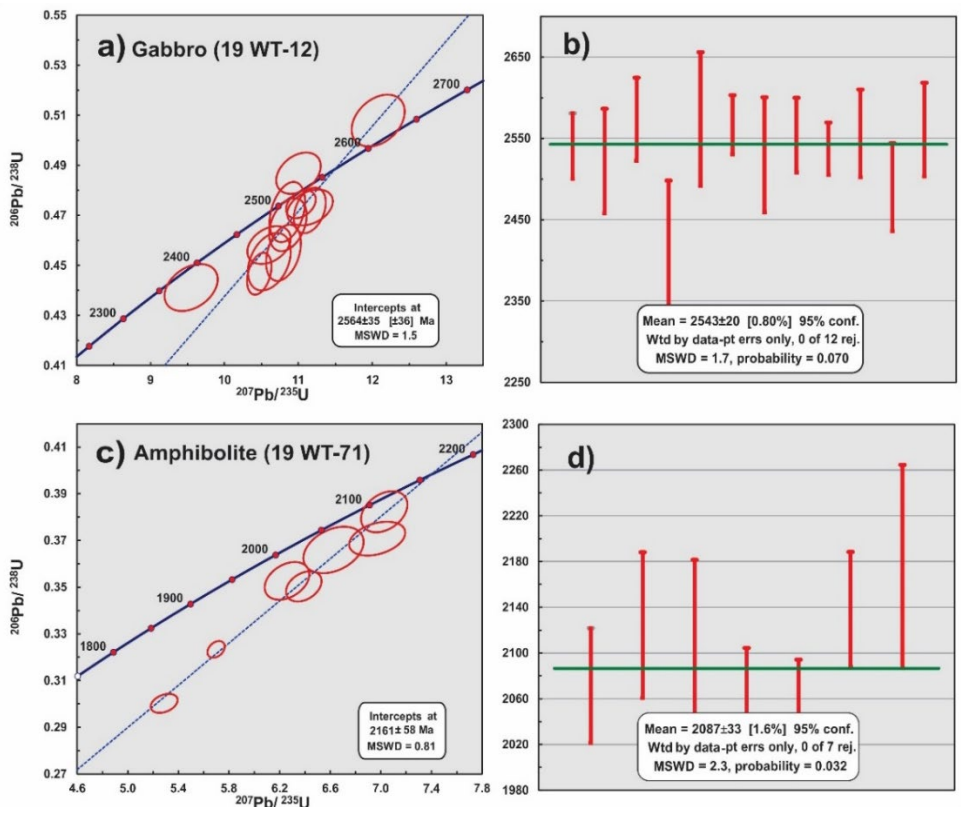

Figure 6. LA-ICP-MS zircon U–Pb Concordia diagrams and weighted average ages. **(a–b)** Gabbros and **(c–d)** Amphibolites.

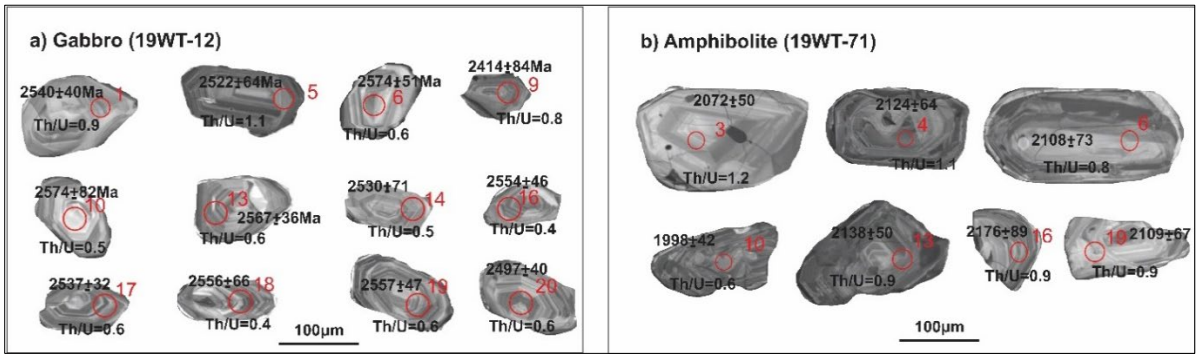

Figure 7. Cathodoluminescence images of representative zircon grains from the **(a)** Gabbro samples and **(b)** Amphibolite samples, where the red circles show the locations of analyzing spots, and the apparent ages of related spots are also mentioned.

The Th/U ratios of the zircons range from 0.6 to 1.2, with most values above 0.7, which is generally characteristic of magmatic zircon. Higher Th/U values (e.g., 1.2) suggest that some zircons retained their original magmatic signatures, while lower values (~0.6) indicate partial metamorphic alteration (Figure 7b). The presence of zircons with a range of ages and slightly variable Th/U ratios suggests that this

amphibolite have experienced a complex geological history, including both magmatic crystallization and later metamorphic events that partially reset the isotopic system. The presence of Paleoproterozoic ages in the amphibolite sample suggests that these rocks represent a metamorphosed mafic intrusion or a basaltic protolith that was subsequently metamorphosed during a Paleoproterozoic tectonothermal event. This event could be linked to large-scale crustal reworking, subduction-related metamorphism, or collisional processes within the North China Craton. The variations in zircon ages within a single sample highlight the importance of U-Pb dating in unraveling the polyphase evolution of ancient mafic units, providing key insights into the geodynamic history of the Wutai Complex.

A mafic magma origin is suggested by these features [74]. Th/U ratios in the range of 0.1 to 1.2 for the zircons suggest a magmatic origin [74]. REE patterns of these zircon grains, distinct positive Ce and negative Eu* anomalies, and a discernible decrease in light REEs relative to heavy REEs further supporting their magmatic origin [75]. Based on these two samples' ages, the gabbros in the Wutai Complex formed in the Late Neoarchean, while the amphibolite formed in the middle Paleoproterozoic.

5.2. Major and trace elements

The Wutai Complex, like other Archean greenstone belts worldwide, has experienced several phases of deformation, metamorphism from greenschist to amphibolite facies, and submarine hydrothermal alteration, which may have contributed to the mobilization of major elements, such as alkali and alkaline earth elements, and may also have impacted the mobility of some trace elements, especially large ion elements with lithophile affinity, such as barium (Ba), strontium (Sr), and rubidium (Rb). As a result, for petrogenetic analysis, the current study focuses on high-field strength elements HFSE (Nb, Zr, Hf, Th, Ti, Y) and rare earth elements (REEs) due to their stability against seafloor alteration and metamorphism [76]. Both gabbros and amphibolites plotted around the tholeiite curve in the AFM diagram. According to the total alkali-silica diagrams (Figure 8), gabbros primarily fall in the basalt field in $Na_2O + K_2O$ *vs* SiO_2 [77] (Figure 9a), while the amphibolites were primarily plotted in the andesite/basalt fields in the $Zr/TiO_2*0.0001$ *vs.* Nb/Y diagram (Figure 9b) [78] Data in the form of grey symbols in the background are from [45]. Geochemistry data of previous studies from the Wutai Complex are mentioned in detail in the Supplementary Table 6.

The elemental compositions of gabbros and amphibolites differ noticeably. The mafic intrusions from the Wutai Complex show distinct geochemical characteristics as briefly explained below.

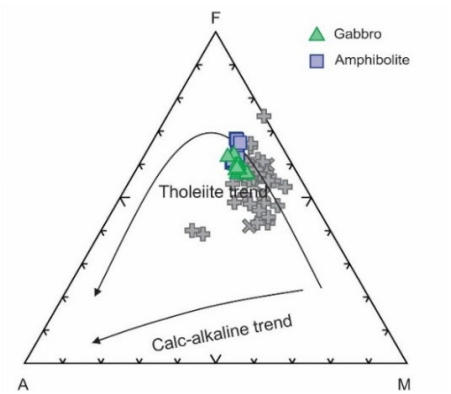

Figure 8. AFM ternary diagram, A = $Na_2O + K_2O$, F = $FeO + Fe_2O_3$ and M = MgO [77]. Data in the form of grey symbols in the background is from [45].

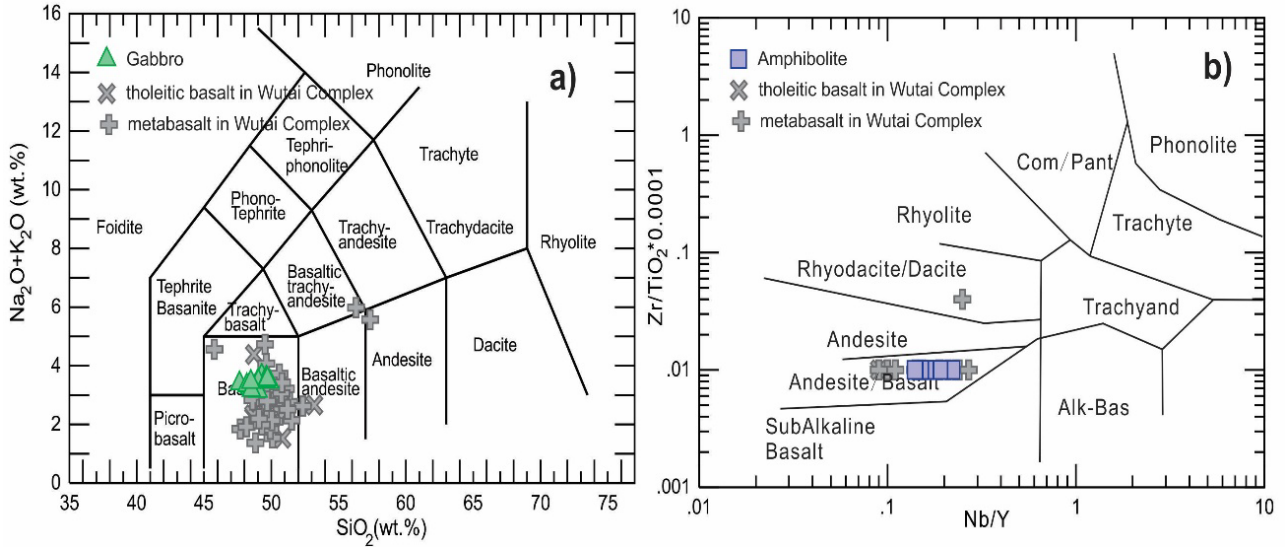

Figure 9. Plots of **(a)** $Na_2O + K_2O$ (wt.%) *vs* SiO_2 (wt.%) [77]; **(b)** $Zr/TiO_2*0.0001$ *vs* Nb/Y diagram [78]. Data in the form of grey symbols in the background is from [45].

5.2.1. Gabbros

The gabbros exhibit higher total REE concentrations (299.81–469.85 ppm) due to their SiO_2 contents in weight percentage, ranging from 47.64 to 49.90 wt.%, MgO content from 4.99 to 7.04 wt.%, K_2O from 0.80 to 1.20 wt.%, K_2O/Na_2O ratios (0.31 to 0.59) and total alkalis ($K_2O + Na_2O$) ranging from 3.14 to 3.65. These gabbros can be categorized as tholeiitic rocks because they have lower LOI values (< 1.3 weight percent) (Supplementary Table 2). In the Rock Chondrite diagram (Figure 10a), the gabbros exhibit a minor abundance of light rare earth elements (LREEs), with variable Eu* anomalies ranging from 2.69 to 4.23 and (La/Yb)n ratios ranging from 7.00 to 8.96. These gabbros show patterns similar to Ocean Island Basalts (OIB) in the primitive mantle normalized trace element pattern (Figure 10b), with a notable enrichment in large-ion lithophile elements (LILE, CS, Rb, Ba, and Th), clear differentiation in high field strength elements (HFSE), and a slight depletion in Nb and Ta.

5.2.2. Amphibolites

The Wutai Complex amphibolites exhibit a range of SiO_2 contents (39.19 to 49.19 weight percent) and MgO contents (5.13–6.53 weight percent). They also have slightly higher K_2O ratios (0.59–1.92 weight percent), which raises the K_2O/Na_2O ratios (0.27–1.26) and raises the concentrations of REE (186.2–218.1 ppm). The data indicate a sub-alkaline basaltic affinity for these amphibolites, which also show higher LOI values (> 1.3 weight percent) (Supplementary Table 3). Additionally, the amphibolites show LREE enrichment in the chondrite normalized REE pattern (Figure 10a). They also have weaker Eu* anomalies between 1.80 and 2.03, lower (La/Yb)n ratios from 2.92 to 5.39 and enrichment in large ion lithophile elements (LILEs), like Rb, Ba, and Cs. The primitive mantle normalized trace element pattern (Figure 10b) displays subduction zone-like patterns for these amphibolites, with characteristic enrichment in large-ion lithophile elements (LILE), distinct differentiation in high field strength elements (HFSE), and evident depletion in Nb, Ta, and Ti anomalies.

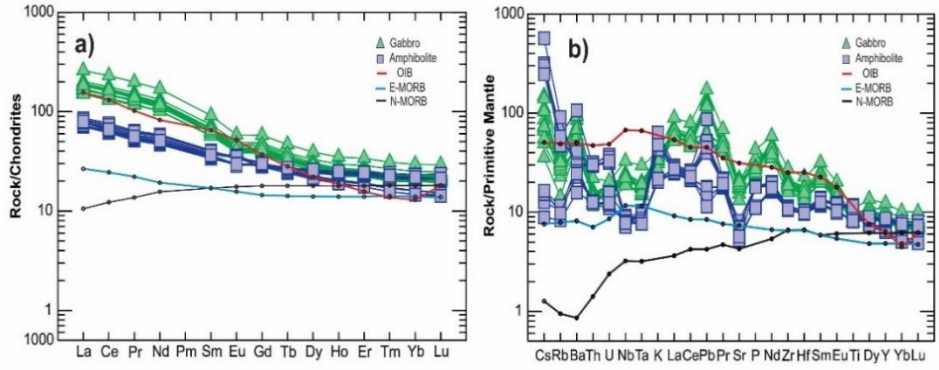

Figure 10. Chondrite-normalized REE patterns and primitive mantle-normalized multi-element diagrams for the mafic rocks of the Wutai Complex, **(a)** Chondrite-normalized REE patterns; **(b)** Primitive mantle-normalized trace element spider diagrams for the Gabbro and Amphibolites. Mantle-normalization values are from [79]. OIB and N-MORB are also shown for comparison.

5.3. Sr-Nd isotope compositions

The gabbro and amphibolite isotopic compositions clearly differ from one another (Figure 11a). With initial $^{87}Sr/^{86}Sr$ of 0.69770 to 0.69930 and consistent Sr-Nd compositions ($\varepsilon_{Nd}(t)$ = 0.9 to 1.2), the gabbros have initial $(^{87}Sr/^{86}Sr)_i$ ratios alternating from 0.70063 to 0.70091 and high $\varepsilon_{Nd}(t)$ values of 4.9 to 6.1 (Supplementary Table 4). In comparison to a normal mid-ocean ridge basalt (MORB), the gabbros have slightly higher initial $^{87}Sr/^{86}Sr$ ratios and higher positive initial $\varepsilon_{Nd}(t)$ values, indicating that they were derived from a depleted mantle domain that was similar to arc basalt but slightly enriched. Positive $\varepsilon_{Nd}(t)$ values and slightly elevated $(^{87}Sr/^{86}Sr)_i$ ratios are consistent with a mantle source influenced by melt metasomatism or slab-derived fluids. However, the isotopic features of the amphibolites are more akin to those of an enriched subduction-modified mantle source. The lower $\varepsilon_{Nd}(t)$ values and depleted HFSE patterns in amphibolites imply that they originated from a mantle source resembling a back-arc basin or a subduction-modified MORB.

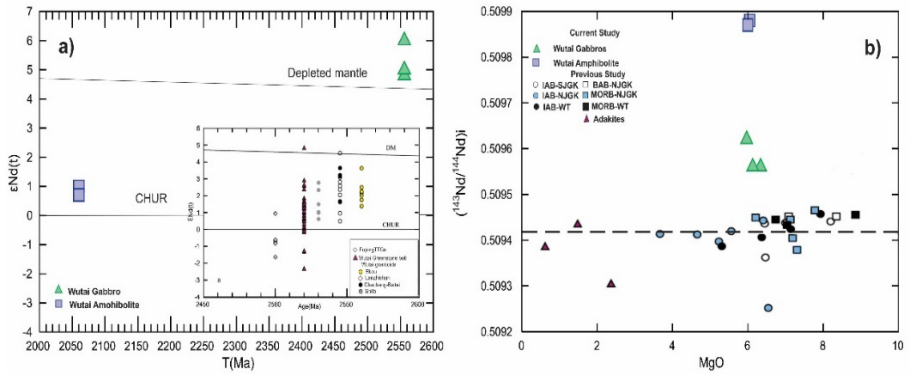

Figure 11. Plots of **(a)** Initial ε_{Nd} (t) value *vs.* age plot illustrates the Nd isotopic variation in the Wutai greenstone belt, Wutai Mafic gabbros, granitoids, and Fuping TTGs. Symbols are Wutai gabbros: green-filled triangles, Amphibolites: Purple-filled squares, MORBs: filled squares; back-arc basin basalts: open squares; arc basalts: filled circles; adakites: filled triangles. Dashed lines indicate the primitive mantle values [79]; N-MORB value from [79]. **(b)** $(^{143}Nd/^{144}Nd)_i$ *vs.* MgO diagram of the Wutai greenstone belt for assessing crustal contamination.

6. Discussion

6.1. Petrogenesis

6.1.1. Alteration effects

The different loss on ignition (LOI) measurements between the gabbros and amphibolites indicate the differences in alteration; the gabbro samples have a lower LOI range of (0.49–1.24 wt.%) (< 1.3 wt.%) and relatively stable concentrations of incompatible elements like Rb (9.8–27.59 ppm), Cs (0.28–1.18 ppm), and K (6640–9960 ppm). It suggests that alteration had a minimal effect on these samples, whereas the amphibolite samples show broader spectrum of alteration, with LOI values for these samples ranged from 0.44 to 5.04 wt.%. The disparities in mobile element ratios, such as K (4897–15936 ppm), Rb (5.27–57.68 ppm), Ba (110.49–741.77 ppm) and Pb (0.8–6.15 ppm), indicates variable degrees of modification, most likely caused by hydrothermal processes. As a result, immobile elements (Ca, Al, and Mg), as well as HFSE and REE, are crucial tools for limiting the petrogenesis of the gabbros, as will be covered in later [10,80].

6.1.2. Fractional crystallization and crustal contamination

The differences observed between the amphibolites and gabbros point to different processes of mineral accumulation or fractional crystallization. MgO, TiO_2, and Fe_2O_3 correlations suggest that olivine separation occurs within the gabbros. The variable relationship of MgO with Al_2O_3 reflects a more complex fractionation process that likely involves multiple phases, including plagioclase, influencing Al_2O_3 concentrations. Variations in K_2O may be attributed to alkali feldspar or other K-bearing minerals. Meanwhile, the correlation between MgO and CaO points to the segregation of clinopyroxene.

Positive correlations between Al_2O_3, TFe_2O_3, and TiO_2 are observed in the amphibolites, indicating that biotite or hornblende are incorporated into minerals during magma crystallization (Figure 12c–f). The inconsistency in the correlation with CaO indicates that the crystallization sequence changed or that multiple mineral phases were involved in influencing calcium levels.

The crystallization and separation of plagioclase from the melt caused the remaining magma to become enriched in calcium and aluminum, resulting in greater concentrations of Al_2O_3 and CaO as compared to the MgO in the ultimate rock composition. Selective separation of plagioclase can be suggested by the strong correlation between CaO, or Al_2O_3 and MgO, in diagrams of both rock types. The negative europium (Eu*) anomalies in amphibolites as compared to the gabbros (Figure 12b), additionally supporting the idea of plagioclase separation. The combined effects of fractional crystallization and the crustal contamination (AFC) are vital in magma derivation, changing both its elemental and isotopic signatures. Geochemical data show that clinopyroxene and plagioclase dominate the crystallization process in gabbros, while plagioclase and hornblende play a key role in the differentiation of amphibolites. Both rock types also show some indications of Fe–Ti oxide separation [81]. Crustal materials usually have low levels of P_2O_5 and TiO_2, but are rich in large ion lithophile elements (LILE), as well as K_2O and Na_2O. So, an increase in the levels of Na_2O, K_2O, LILE, and a decrease in P_2O_5 and TiO_2 suggest crustal contamination. The correlation between TiO_2 and MgO in both rock types indicates that crustal contamination and fractional crystallization occurred besides (Figure 12f). The spider diagrams

for gabbros show slight positive Zr–Hf anomalies, which suggest the possibility of crustal contamination. Although crustal materials typically exhibit elevated Th concentrations, the analyzed gabbros display consistently low Th abundances, diminished Th/Yb ratios, and elevated Nb/Th values. In contrast, amphibolites are characterized by further reduced Th/Yb ratios, marginally higher Th contents, and similarly high Nb/Th ratios. Both lithologies demonstrate geochemical signatures indicative of crustal contamination processes.

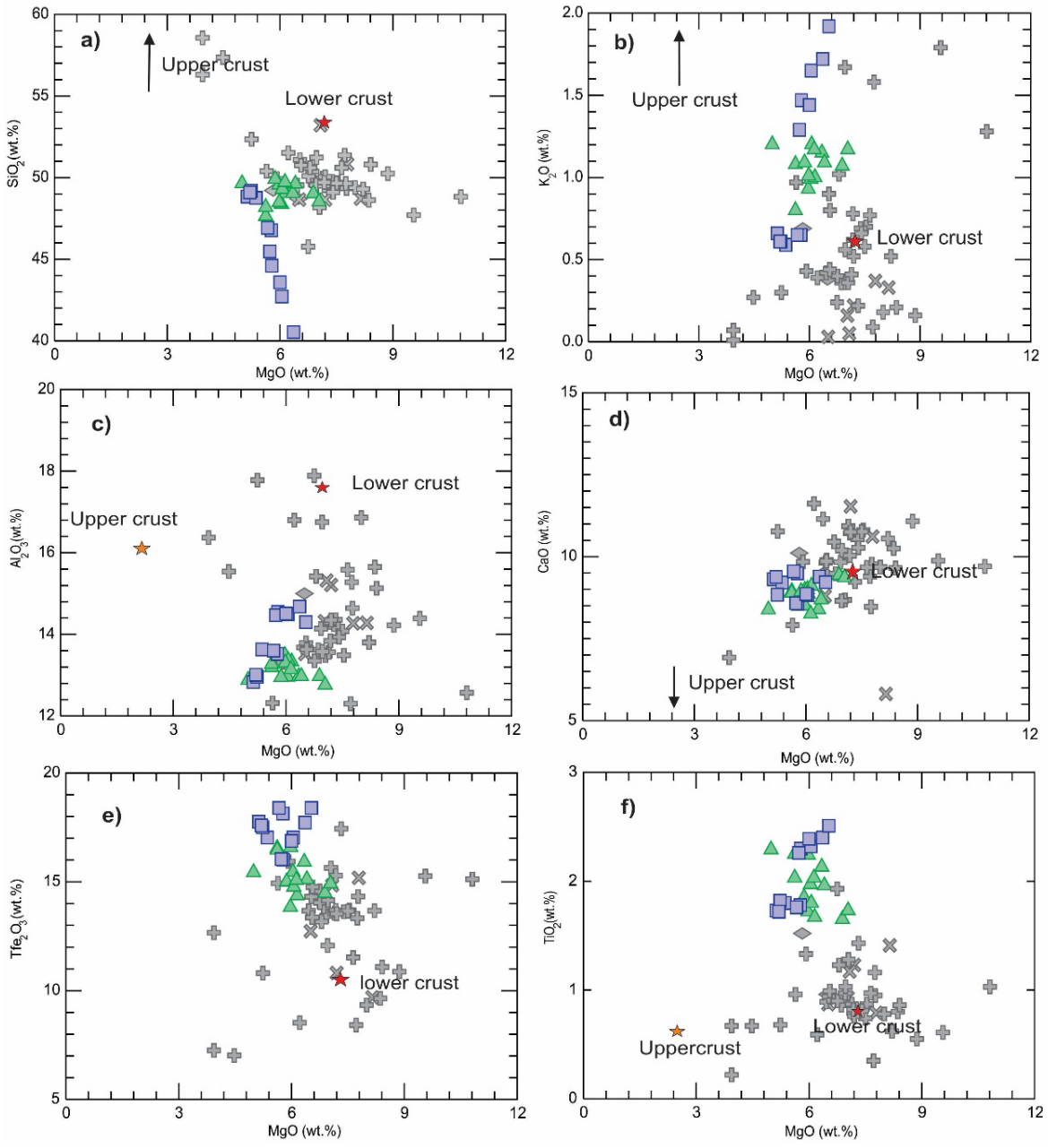

Figure 12. Harker diagrams for the gabbroic Mafic Rocks in Wutai Complex, NCC, China.

In terms of geochemistry, gabbros contain (19.44–23.40) ppm of Nb–Ta, (40.60–44.29) ppm of Zr–Hf, (10.60–13.49) ppm of Nb/Th ratios, (0.30–0.41) ppm of Th/Yb ratios, (1.02–2.71) ppm of Th levels, and (3.12–12.25) ppm of Pb (Supplementary Table 2). The amphibolites have Zr–Hf concentrations of (39.19–40.09) ppm, Nb–Ta levels of (12.10–18.40) ppm, Nb/Th ratios of (1.87–5.83) ppm, Th/Yb ratios

of (0.28–1.03) ppm, Th concentrations of (1.02–2.71) ppm, and Pb levels of (0.81–6.51) ppm (Supplementary Table 3). Although, high Pb levels indicate some contamination occurred, the gabbros, with their slightly high Nb–Ta and Nb/Th ratios, indicate a little crustal contamination in their mantle source, while amphibolites, with their wider Th/Yb ratios and lower Nb–Ta and Nb/Th ratios, show more obvious signs of crustal contamination. However, their relatively lower Pb concentrations in comparison to gabbros suggest a different nature or source of crustal contamination. In order to ascertain the possible influence of crustal contamination on isotopes, we examined the correlation between isotopic ratios and differentiation metrics like MgO (Figure 11b). The negative correlation among $(^{143}Nd/^{144}Nd)_i$ and MgO and the relatively low $(^{143}Nd/^{144}Nd)_i$ (~0.5098) compared to mantle-derived magmas (e.g., MORB) suggests that continental crust had a major impact on the Wutai gabbros initial magmas during intrusion (AFC process) [25].

6.1.3. Nature of the mantle source

Heavy rare earth elements (HREE) and high-field strength elements (HFSE) distribution is controlled by partial melting processes [82]. These components are essential for determining how much of the source has been depleted [83]. In the Arc-back-arc basin settings, high-field strength elements are useful for determining mantle source characteristics that might have been impacted by previous melting events [83,84]. Previous studies indicate that clinopyroxene exhibits different Nb–Ta and Zr–Hf partitioning than anhydrous silicate melts [85,86].

In the clinopyroxene melt system, zircon shows significantly lower incorporation into the melt compared to hafnium, suggesting that zircon remains solid during melting. The incompatibility factor of 1.5 to 2 indicates the strong preference of hafnium in the melt. In contrast, Nb is more compatible than Ta, as evidenced by an Nb/Ta ratio below 1, which means Nb is more readily incorporated into the melt. These differences in element behavior during partial melting can affect the geochemical properties of the resulting magma. Consequently, during upper mantle melting, the Zr/Hf and Nb/Ta ratios clearly separate and frequently show a positive correlation. These ratios may be preserved by arc-related basalts from a mantle wedge, which show different levels of mantle depletion before melt production [87]. Arc volcanic rocks with low Nb/Ta ratios indicate that melts from the mantle wedge have previously been extracted (Figure 13a–d). This suggests a melt removal process that occurred in the mantle prior to the formation of volcanic rocks, which is thought to be typical of subduction-related environments [88]. Sub-chondritic Nb/Ta ratios are expected to positively correlate with a number of other elemental ratios, including Th/Yb, Zr/Ti, La/Yb, Zr/Yb, Y/Sc, and Ti/V. These proportions typically fall with increasing mantle wedge depletion, suggesting a connection between the resultant rocks' elemental compositions and the degree of mantle depletion [82,88]. From the rare earth elements (REE's), the degree of partial melting and the mantle source composition can be assumed.

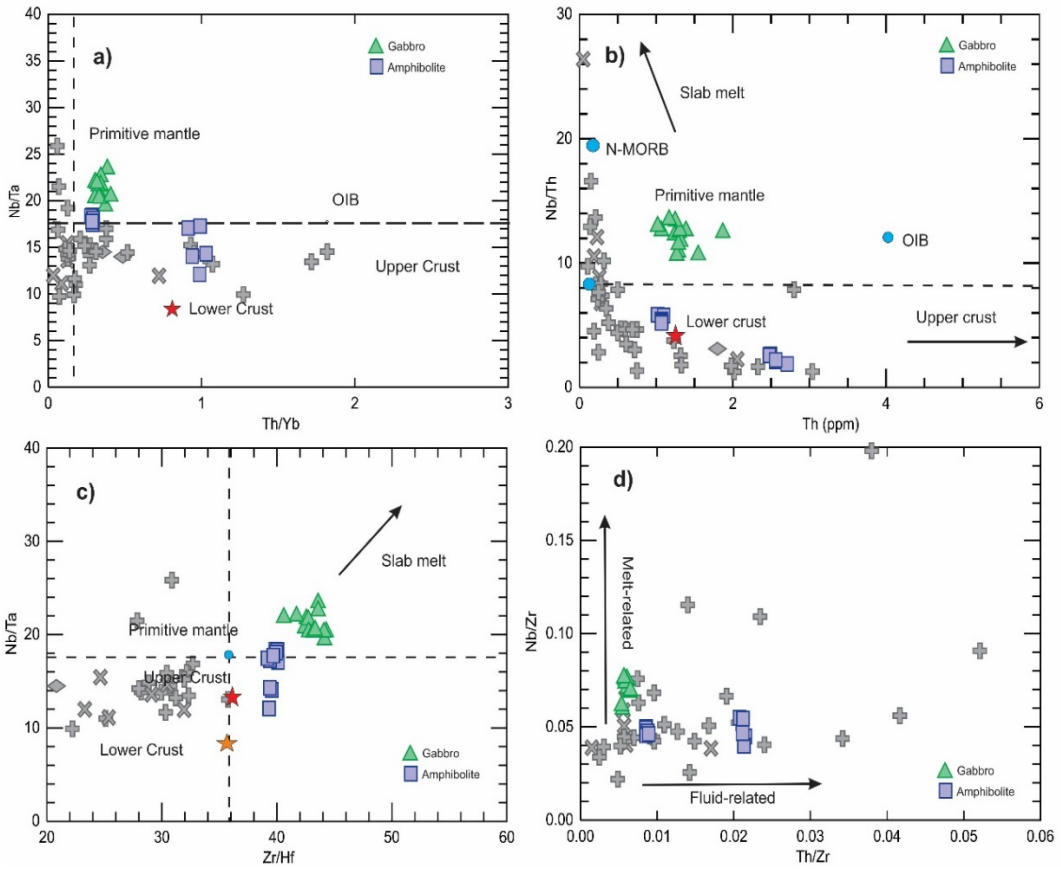

Figure 13. Plots of **(a)** Nb/Ta *vs.* Th/Yb; **(b)** (Nb/Th) *vs.* (Th) ppm; **(c)** (Nb/Ta) *vs.* (Zr/Hf); **(d)** Nb/Zr *vs.* Th/Zr [89]. Values of N-MORB, OIB, and primitive mantle are from [79]. Values for the upper and lower crust are from [90].

The Sm/Yb ratios are comparatively stable in the presence of partial melting in a spinel herzolite mantle source because the partition coefficients of the two elements are comparable. However, this melting process can lead to a decrease in La/Sm ratios and lower concentrations of Sm in the resulting melts, indicating how the melting dynamics influence the elemental composition of the gabbros [91]. Therefore, it is expected that melt sources derived from spinel lherzolite will have melting tendencies that are almost equal and consistent with a mantle array characterized by compositions ranging from depleted to enriched sources [92]. The partial melting of garnet-lherzolite will, however, produce a steeper trend on a Sm/Yb *versus* Sm diagram than the melting of spinel lherzolite because garnet has a substantially higher partition coefficient for Yb ($D_{garnet/melt}$ = 6.6) than Sm ($D_{garnet/melt}$ = 0.25) [93]. The Sm/Yb ratios in the Wutai gabbros exceed those predicted by the spinel-lherzolite melting curve but remain lower than values associated with the garnet-lherzolite melting trend. The samples analyzed in the current study fall in the transition range between two curves on the spinel-garnet-lherzolite (50:50) melting path (Figure 14a,b). The Sm/Yb vs La/Sm diagram displays that the samples are positioned near the spinel + garnet lherzolite mantle source. The high Sm/Yb and La/Sm ratios in the gabbro samples point to a mantle source that syndicates both garnet-lherzolite and spinel characteristics, suggesting that their parental magmas originate from an area near the spinel-garnet lherzolite melting curve. While the amphibolites plotted in the pure spinel lherzolite and spinel-garnet lherzolite regions (Figure 14b) indicate different partial melting depths or different mantle sources, the increased Sm/Yb and La/Sm ratios in the gabbros propose

a mantle source that blends characteristics of garnet and spinel lherzolite, suggesting that their parent magma originated from a source region of spinel-garnet lherzolite. In general, the geochemical data, particularly the ratios of Sm, Sm/Yb, and La/Sm, indicate that these gabbros and some of the amphibolites originate from a mantle source that switches between garnet and spinel lherzolite facies, suggesting melting at different levels. This shows complications of their mantle source and the mantle melting processes that contribute to these gabbros, and amphibolites close to the spinel lherzolite curve most likely originate from a shallower mantle region that is primarily composed of spinel lherzolite.

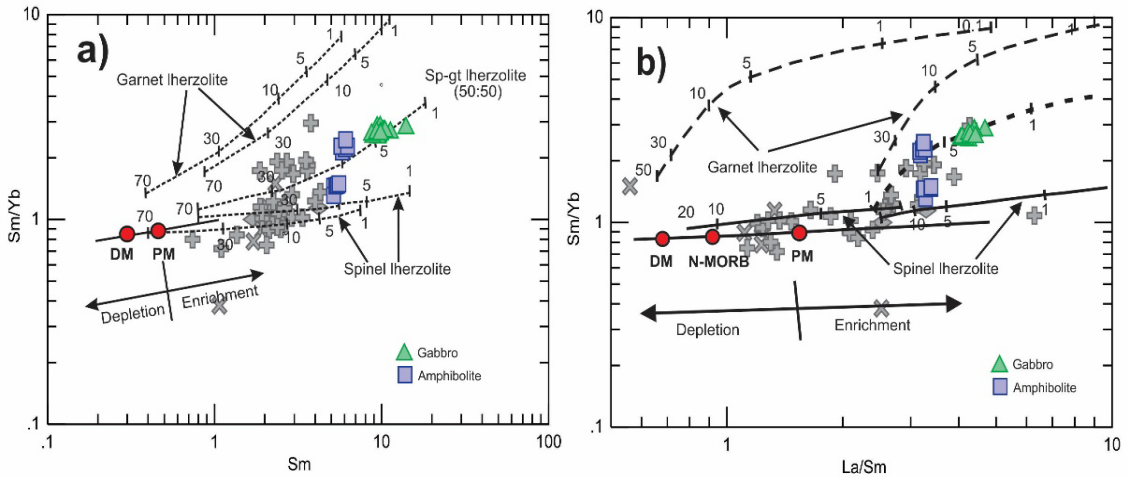

Figure 14. Plots of **(a)** Sm/Yb *vs.* Sm, and **(b)** Sm/Yb *vs.* La/Sm. Mantle array (heavy line) is defined by depleted MORB mantle, DMM [94], and primitive mantle (PM [79]). Melting curves for spinel lherzolite (Ol53 + Opx27 + Cpx17 + Sp11) and garnet peridotite (Ol60 + Opx20 + Cpx10 + Gt10) with both DMM and PM compositions are after [91]. Numbers along lines represent the degree of the partial melting.

The gabbros have relatively low initial $^{87}Sr/^{86}Sr$ ratios (0.70466–0.70677) and $\varepsilon_{Nd}(t)$ values ranging from 4.9 to 6.1, suggesting a relatively juvenile, depleted mantle source with little crustal contamination. On the other hand, the amphibolites show higher initial $^{87}Sr/^{86}Sr$ ratios (0.721109–0.722678) and $\varepsilon_{Nd}(t)$ values between 0.9 and 1.2, suggesting an enhanced mantle source that has been greatly impacted by subduction-related processes (Supplementary Table 4). The isotopic compositions and trace element ratios of the rocks provide important information about the characteristics of their mantle source area. The incompatible trace element ratios of Nb/Th and La/Sm, in particular, and the different initial $^{87}Sr/^{86}Sr$ ratios indicate that the gabbros and amphibolites did not form from a similar parental magma through assimilation and fractional crystallization processes alone, but rather originate from separate parental melts. In addition to higher concentrations of Zr (177–308 ppm), TiO_2 (1.65–2.29 wt.%), P_2O_5 (0.52–0.9 wt.%), and Nb (13.3–23.3 ppm), the gabbros also exhibit elevated $(Nb/Th)_{PM}$ (10.62–13.49), $(Nb/La)_{PM}$ (0.31–0.40), and Nb/U (38.8–54.4), all of which point to an enriched mid-ocean ridge basalt (Supplementary Table 3, Figure 15a–d). These geochemical characteristics indicate a signature of Nb-enriched basalt-andesites (Figure 15c,d), as previously defined in the literature [95–97]. Three possible scenarios have been presented to explain the formation of Nb-enriched basalt-andesites: (1) partly melting the subducted plate, (2) partially melting the oceanic island basalt (OIB), or (3) mantle metasomatism by adakitic melts [95,98–100]. Additionally, the MgO content ranging from (4.99–7.04 wt.%), Cr (126–354 ppm), and Ni (72–134 ppm),

further supports a mantle-derived origin consistent with an E-MORB. The relatively high Nb/Zr and low Th/Zr ratios reflect mantle heterogeneity or the influence of enriched components in the source [101] (Figure 13d). The geochemical ratios of the amphibolites reveal important details about their magma genesis and mantle source characteristics. The elevated TiO_2 (1.72–2.5 wt.%) and Zr (117–129 ppm), coupled with lower P_2O_5 (0.24–0.41 wt.%) and Nb (5.07–6.38 ppm), indicate a mantle source influenced by residual phases like rutile or ilmenite, which retain HFSE such as Nb and Ta. This depletion of Nb, along with enriched Zr, is consistent with a subduction-modified mantle, where slab-derived fluids or melts selectively enrich LILE and LREE while depleting HFSE. Higher $(Nb/Th)_{PM}$ (1.87–5.83) and lower $(Nb/La)_{PM}$ (0.25–0.37) ratios reflect a source enriched in Nb relative to Th but depleted in Nb relative to La, typical of subduction processes that retain Nb in residual phases. Similarly, low Nb/U ratios (6.7–26.0) point to crustal contamination or slab-derived enrichment, as subducted sediments and slab fluids are rich in U but depleted in Nb.

The relatively lower Nb/La (0.25–0.37) ratios further support subduction influence, while the higher Ce/Pb ratios (7.60–50.12) suggest limited sediment contribution and dominant metasomatism by slab-derived fluids. Together, these features imply that the amphibolite magmas originated from a subduction-modified mantle wedge, enriched by slab fluids or melts, with HFSE depletion and heterogeneity in the degree of metasomatism, consistent with arc or back-arc tectonic settings. The lower Nb/Zr ratio also implies a mantle source that experienced selective depletion of Nb due to slab-derived fluids or melts, pointing to subduction-related metasomatism (Figure 13d). This suggests that the amphibolites experienced a more complex metasomatic history than the gabbros, likely involving both adakitic melts and slab-derived fluids. Therefore, the amphibolites underwent a more mixed process of metasomatism including both adakitic melts and fluids, whereas the Wutai Nb-enriched gabbros were most likely generated by partial melting of a mantle wedge metasomatized by adakitic melts with minimal contributions from slab-derived fluids.

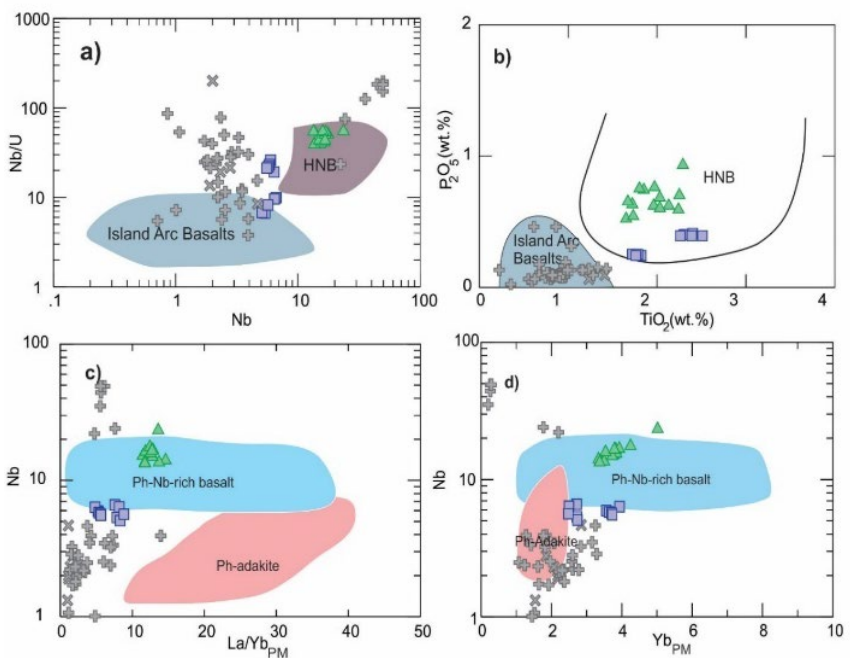

Figure 15. Plots of **(a–b)** Nb/U *vs.* Nb and P_2O_5 (wt.%) *vs.* TiO_2 (wt.%) diagram (after [95]); **(c–d)** $(La/Yb)_{PM}$ *vs.* Nb and Yb_{PM} *vs.* Nb diagrams (after [102]).

According to [103,104], trace element ratios like Ba/Th, Rb/Th, and Cs/Th were analysed to determine the composition of aqueous fluids in order to distinguish between shallow aqueous fluid contributions and deeper sediment melt components. The increase of La and higher La/Sm ratios in these rocks suggest the involvement of sediment-derived melts, a hallmark of subduction zone magmatism where subducted sediments significantly contribute to magma generation (Figure 16a–d). Both the studied gabbros and amphibolites align with the compositional ranges of arc and back-arc basin (BAB) environments. The gabbros display higher La/Sm ratios, indicating a stronger affinity with subducted sediment-derived melts, while the amphibolites exhibit marginally raised Rb/Th and Cs/Th ratios, demonstrating enrichment by sediment melts and aqueous fluids that are high in Ba, Rb, and Cs. This suggests that the mantle sources of these rock types were metasomatized by subduction components, with the gabbros showing a greater influence of deep sediment melts and the amphibolites reflecting the impact of shallow aqueous fluids.

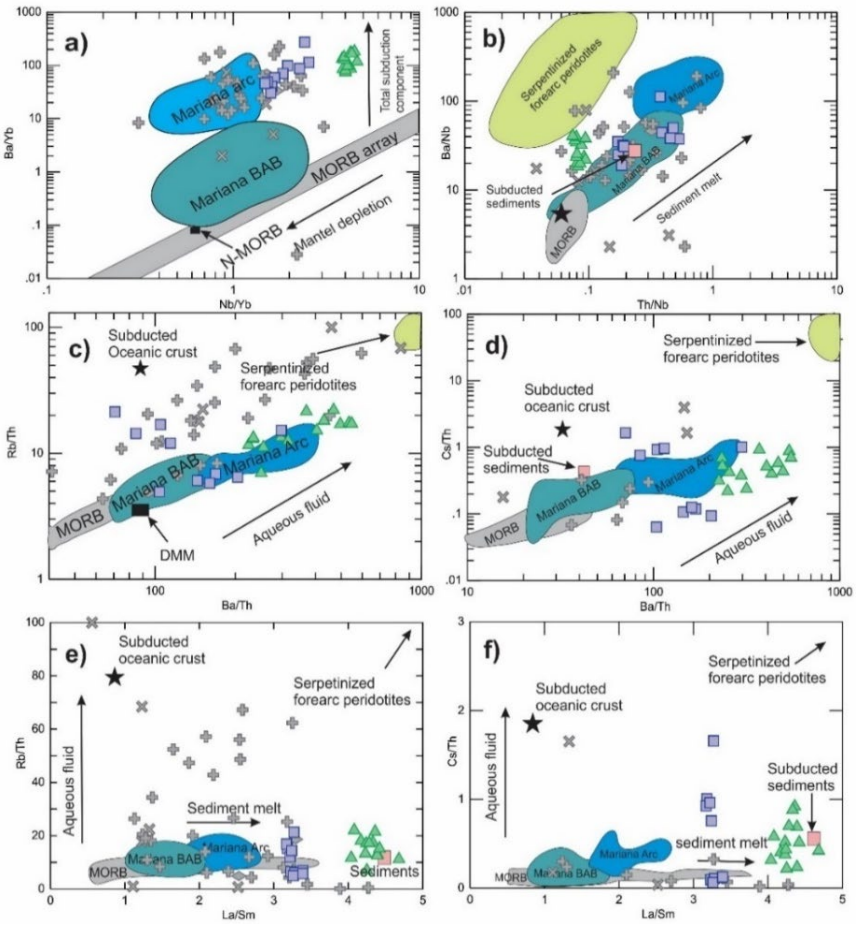

Figure 16. Plots of **(a)** Ba/Yb *vs.* /Yb, **(b)** Ba/Nb *vs.* Th/Nb, **(c)** Rb/Th vs Ba/Th, **(d)** Cs/Th *vs.* Ba/Th, **(e)** Rb/Th *vs* La/Sm and **(f)** Cs/Th *vs.* La/Sm [105]. N-MORB, OIB, and primitive mantle are from [79].

6.1.4. Mantle enrichment through slab-derived fluids and melts

Subduction components can be reliably assessed using ratios of fluid/melted-mobile elements from the slab, such as Cs, Rb, Th, Ba, and La, to fluid-immobile elements from the slab, such as Nb, Ta, Yb, and

Sm [104]. Aqueous fluids and deeper sediment melts carry Ba, Cs, and Rb [104,106,107]. The Ba/Nb and Ba/Yb ratios show the overall subduction constituents (Figure 16a,b), whereas the La/Sm and Th/Nb ratios show the influence of deeper sediment melts, while the Ba/Th, Cs/Th, and Rb/Th ratios highlight the input of shallower aqueous fluids in mobilization. However, sediment melts primarily mobilize La and Th [105]. In the Ba/Nb *versus* Th/Nb diagrams, the compositional range of Mariana BAB lavas clearly illustrates the influence of deep sediment melts in the amphibolites, and both the gabbros and amphibolites show elevated Ba/Yb ratios, placing them above the MORB array and showing an upward trend [104,108]. These observations suggest the involvement of a subduction component. The compositional range of Mariana BAB lavas in the Ba/Nb *vs* Th/Nb diagrams amply demonstrates the impact of deep sediment melts in the amphibolites [109,110]. Shallower aqueous fluids may be involved if Ba increases without Th rising in tandem. The amphibolites having higher Th/Nb ratios suggest that their formation was near the trench, and also indicate the high fluid impact from the subducting slab. On the other hand, the gabbros having low Th/Nb ratios suggest most likely formed farther away from the trench, which means that these fluids had less of an impact. Both kinds of rocks have BAB-like Rb/Th, Th/Nb, Cs/Th, and La/Sm ratios, which indicate that sediment melts interacted with their mantle sources (Figure 16b,e,f). The high La/Sm ratios also suggest a noteworthy input from melts originating from sediments, suggesting that the parental magmas of these gabbros included elements from subducted sediments, which are comparatively rich in La as opposed to Sm. Amphibolites have noteworthy LILE enrichment (e.g., Ba/Zr (0.91–6.20), Ba/Nb (19–112), Ba/Th (70–298)), indicating hydrous fluid enrichment, and other geochemical characteristics typical of back-arc settings. They have variable Rb/Y (0.14–1.93) and low Nb/Zr (0.04–0.06) ratios, which are similar to Kamchatka arc rocks and indicate that fluids driven by slab modified the mantle source [89]. The high K/Rb ratios and low Th/Zr support the idea that fluids from the slab have changed the mantle source considerably, and that fluids from the subducted slab have influenced the geochemistry of the mantle wedge above as well as lowering the melting point of peridotite, which encourages the formation of subduction-related magmas [111,112]. The high K/Rb and low Th/Zr ratios indicate that fluids input from the slab play their role in changing the mantle source.

The Wutai gabbros, which have moderately positive Zr–Ta and Nb–Ta anomalies, as well as super-chondritic Nb/Ta (19.44–23.40) and Nb/Th (10.62–13.49) ratios, demonstrate negligible slab-derived fluid's interaction with; their low Th/Yb ratios (0.30–0.41) further support limited thorium addition, while amphibolites exhibit more variable lower Nb/Th (1.87–5.83) ratios, and Nb/Ta (12.40–18.40), indicating greater Th enrichment but less influence from Nb-rich slab fluids. The Zr/Hf ratios in both gabbros (40.60–44.29) and amphibolites (39.19–40.09) are near chondritic, which specifies limited fractionation between Zr and Hf, and represents that processes like partial melting or crystallisation have not significantly influenced these ratios. Since the mantle source may have undergone dilution or depletion prior to the formation of the gabbros, the low concentrations of Rb and Th in the gabbros reflect their true characteristics. As proposed by [53], the inclusion of low K and Rb and low-Th constituents is likely to result in dilution. Additionally, partial melting of the subducted slab may result in elevated K/Rb ratios in the melt but low K and Rb contents because the large ion lithophile elements (LILE) were depleted during earlier slab dehydration [113]. While magmas with constant K/Rb ratios are linked to enrichment through fluids [53], high K/Rb magmas are typically linked to enriched source through melting. The high K/Rb ratios in the gabbros suggest that their source was significantly altered by

melting processes, and as mentioned above, Nb/Ta ratios are crucial markers for identifying magma source modification by fluids or melts [42,114]. In general, gabbros have higher Nb/Ta ratios than amphibolites (Figure 13a,c). They also have higher Nb/Zr (0.06 to 0.08) and Nb/Y (0.34 to 0.42) ratios, but lower Rb/Y (l0.68) and Th/Zr (below 0.01) ratios. Conversely, amphibolites have lower Nb/Zr (0.04–0.06) and Nb/Y (0.14–0.22) ratios, as well as higher Rb/Y (up to 1.93) and Th/Zr (below 0.02) ratios. These features are similar to those of northern Kamchatka lavas, which are formed by the interaction of sub-arc mantle peridotites with melts derived from siliceous slabs [89,115]. Different degrees of involvement from melts and fluids derived from subducted slabs are indicated by the distinctions in chemical composition between gabbros and amphibolites. Gabbros show increased Nb/Ta, decreased Rb/Y and Th/Zr ratios, and increased Nb/Zr and Nb/Y ratios, indicating that slab-derived materials have had little effect. On the other hand, amphibolite's geochemical ratios show a greater impact from fluids and melts derived from slabs. These variations demonstrate the complex interaction between subduction-related influences and mantle processes in the formation of these rock types.

6.2. Late Paleoproterozoic tectonic setting of the TNCO

The Late Paleoproterozoic tectonic evolution of the Trans-North China Orogen (TNCO) is constrained by geochronological and structural evidence from the Wutai, Fuping, and Hengshan complexes in the previous research. The Wutai Complex hosts Paleoproterozoic granitoids, including the 2176 ± 12 Ma Dawaliang pluton, and the 2117 ± 17 Ma Wangjiahui pluton's pink phase. Syn-tectonic mafic dykes, emplaced in back-arc or intra-arc settings, yield a SHRIMP age of 2147 ± 5 Ma [116]. The overlying Hutuo Group, unconformably overlying the Wutai and Fuping complexes [31,71] shares metamorphic and deformational patterns with the Upper Wutai Subgroup. The felsic metamorphosed volcanic tuffaceous rock from the Hutuo Group encompasses 2180 ± 5 and 2087 ± 9 Ma SHRIMP $^{207}Pb/^{206}Pb$ ages, respectively [31].

The Palaeoproterozoic Nanying granitic gneisses are widely distributed in the Fuping Complex. SHRIMP data demonstrate that these Nanying gneissic granites were likely emplaced to some extent further ahead than the Dawaliang granites in 2077–2024 Ma [117,118]. References [12,13] identified Paleoproterozoic gneissic granites by means of the single-grain evaporation and SHRIMP procedures and documented their emplacement at c. 2360 Ma, 2330 Ma, and 2250 Ma, consecutively. These ages suggest that the main tectonic activity in the Hengshan-Wutai-Fuping belt took place in the Palaeoproterozoic era rather than in the Late Archaean era [71]. Furthermore, in the Fuping Complex [119], considered age of the Wanzi supra crustal assemblage between 2800 and 2560 Ma. Reference [118] analyzed two Al-rich gneiss samples from the Wanzai assemblage and attained SHRIMP $^{2o7}Pb/^{2o6}Pb$ zircon ages of 2502 Ma and 2507 Ma. Reference [117] marked SHRIMP zircon age of 2097 Ma, from the Wanzi paragneiss. Reference [120] employed the LA-ICPMS technique on sillimanite paragneiss and obtained three upper concordia intercept ages of 2099 ± 22 Ma, 2110 ± 30 Ma, and 2112 ± 23 Ma from the Wanzi supracrustal.

The current study, following the acquisition of our new LA-ICPMS zircon ages 2161 ± 58 Ma to 2087 ± 33 Ma combined with whole-rock geochemistry, and isotopic analysis of the Wutai Amphibolites support a back-arc basin (BAB) setting in the Paleoproterozoic, consistent with granitoid and gneiss studies across the Fuping, Hengshan, and Hutuo units (Supplementary Table 5). Additionally, based on our new results and interpretations, we proposed a tectonic model of the Paleoproterozoic evolution of the Wutai Complex, which gives new evidence for the Late Paleoproterozoic tectonic evolution of the TNCO.

7. Implications for the onset of plate tectonics

The Neoarchean tectonics of Wutai Complex is pivotal in comprehending the tectonic history of the Hengshan–Wutai–Fuping region. The geochemical characteristics of Wutai meta-volcanic rocks are widely recognized as key indicators of subduction processes [5,18,57,68,70]. References [25,45] suggested that the occurrence of MORB, BABB, and IAB-type meta-basalts within the Shizui and Taihuai Subgroups of Wutai meta-volcanic rocks formed in a back-arc basin environment. According to [121] the Neoarchean to Paleoproterozoic evolution history of the NCC especially in the TNCO can be divided into four stages: ~2.58–2.45 Ga initial Cratonization, ~2.50–2.45 Ga post-collisional magmatism, two subduction-rift periods ~2.45–2.12 Ga and 2.12–1.98 Ga subduction rift periods, and ~1.96–1.80 Ga East block and West block amalgamation. Whereas reference [122] alienated Wutai arc magmatism into two separate pulses, the 2560 to 2540 Ma, Lanzhishan, Chechang-Beitai, Longquanguan granitoids and Ekou, granites, represent the early phase, and the ca. 2170 Ma and 2000 Ma Wangjiahui granite and Dawaliang represent the later phase. The subduction and arc magmatism-related felsic volcanics of the Wutai Complex yielded ca. 2540–2515 Ma ages. Reference [123] on the basis of 2137 ± 9 Ma Wutai Huangjinshan porphyry granites proposed that the 2.2–2.0 Ga was a rifting stage in the NCC. Reference [30] reported zircon U-Pb ages of the Wutai greenstone, volcanic tuff, phyllite, and BIF, and presented that the during 2.87–2.45 Ga, Wutai arc was fabricated. Furthermost, reference [8] divided the evolution history of the Wutai arc into four steps on the basis of U-Pb ages: (1) Subduction initialization based on 2800 Ma zircon grains obtained from metasedimentary rocks; (2) Arc-accretionary complex based on 2750–2300 Ma, voluminous volcanic rocks and ca. 2600 to 2400 Ma with the granitoids, with a peak at 2529 Ma, considered as the main phase of subduction-related arc magmatism; (3) Back-arc rift setting: based on ca.2300 Ma to 2100 Ma granitoids with a peak at 2127 Ma. According to [73] (ca. 2300–2100 Ma), Paleoproterozoic granitoids belong to the back-arc rift setting in the Wutai Complex; (4) Arc-continent collision: amalgamation of the East block and West block occurred around ca. 1900–1750 Ma, [1,124,125], assembly of Hengshan, Wutai, and Fuping complexes. The magma mixing between subduction-related melts and back-arc basin-derived melts occurs because of mantle upwelling. The accumulation of the Wutai intra-oceanic arc-back arc is undertaken due to the closure of the back-arc basin owing to subduction and accretion progressions [126,127]. The Hengshan, Wutai, and Fuping Complex may indicate a portion of several arc systems or a mix of island arc-back arc wreckages interspersed with a developing magmatic arc arrangement along the western margin of the eastern block of the North China Craton [13,31]. The NCC preserves some of the oldest rocks on Earth, with zircon U-Pb ages dating back to ~3.8 Ga [128,129]. This places it among the oldest cratons, comparable to the Isua Greenstone Belt in Greenland (~3.7–3.8 Ga) and the Acasta Gneiss Complex in Canada (~4.0 Ga) [130]. However, the NCC is distinct in its prolonged and complex tectonic history, involving multiple episodes of crustal growth, reworking, and metamorphism during the Archean and Paleoproterozoic [131]. Much of the juvenile crust of the Hengshan–Wutai–Fuping belt was accreted in the period ~2.5~2.4 Ga, though several magmatic accretionary events occurred during Late Archean to Paleoproterozoic times. However, more than 90 % of juvenile crust in other complexes (e.g., the Luliang, Zhongtiao, Northern Hebei complexes) in the Trans-North China. Orogen was added in the period 2300–1900 Ma [69]. This suggests that the Trans-North China Orogen records magmatic-tectonic evolution lasting for nearly 650 Ma.

The Neoarchean to the Paleoproterozoic Nb-enriched gabbros and amphibolite rocks analyzed in the current study yielded crystallization ages around 2.56–2.54 Ga and 2.16–2.08 Ga (Figure 6a–d, Supplementary Table 1). The gabbros, with an upper intercept age of 2564 ± 35 Ma and a mean age of 2543 ± 20 Ma, reflect formation during the Late Archean (specifically, the Neoarchean Era). These close ages suggest a single magmatic event with minimal alterations post-crystallization. The upper intercept age likely marks the initial crystallization and emplacement, while the mean age could represent later cooling or minor post-crystallization adjustments, potentially due to low-grade metamorphism or Pb loss. This setting aligns with typical Neoarchean tectonic environments along the Wutai Complex, which were characterized by significant continental crustal growth and stabilization. Taking into account the subduction-related intrusions in the Wutai Complex, these ~2.56 Ga Nb-enriched gabbros show subduction signatures, suggesting their derivation by partial melting of a mantle wedge metasomatized by adakitic melts with minor contributions from slab-derived fluids. This suggests that tectonic activity in this setting enabled the formation and emplacement of gabbros-rich mafic magmas by oceanic subduction, forming part of the foundational crustal architecture during the Late Archean (Figure 18a), which implies that plate tectonics at least partly happened, most likely in the latest Neoarchean.

The upper intercept age of 2161 ± 58 Ma and the mean age of 2087 ± 33 Ma place amphibolites in the Paleoproterozoic Era, specifically the Orosirian Period. The period associated with post-orogenic or collisional tectonic settings, as tectonic regimes evolved toward modern-style plate tectonics. This suggests that the amphibolites formed during a later tectonic event, possibly related to post-collisional magmatism or the stabilization of crust after a significant orogeny. The gap between the upper intercept age (2161 Ma) and mean age (2087 Ma) indicates that the rock underwent some degree of isotopic disturbance and reheating after its initial emplacement because of prolonged cooling and metamorphic overprinting during subsequent tectonic events. The presence of hornblende also suggests hydration of the magma, likely due to subduction or fluid-related processes, which are common in convergent tectonic settings or areas experiencing crustal thickening.

Concurrent slab melting and dehydration are indicated by the proximity of gabbros and amphibolites, suggesting a steep subduction zone with a relatively warm mantle. The Wutai area's Late Archean to Paleoproterozoic mafic intrusions lend credence to the complex's multi-stage tectonic and magmatic history. Along the eastern edge of the Western Block, these intrusions are thought to be a component of a magmatic system connected to subduction. Prior studies have demonstrated that the subduction zones' thermal structure has a significant impact on the geochemistry of their magmas [132–134]. The Wutai Complex's gabbros and amphibolites, which were formed over different periods, show trace element patterns typical of igneous rocks related to subduction, with enrichment in large ion lithophile elements (LILEs) and variable depletion in high field strength elements (HFSEs) (Figure 10) [51,54,115,135,136]. An affinity for arc magmas is indicated by the gabbros plotting inside the OIA field boundary [137] in the MnO-TiO_2/10-P_2O_5 diagram following [40] (Figure 17a). A back-arc extension environment (Ti/V = 10–50) is consistent with gabbros and amphibolites, both of which have high Ti/V ratios (23–45) that place them in the MORB-(BAB) field (Figure 17c) [103,138,139]. According to the geochemical data, the Nb-enriched gabbros of the Late Archean were formed from different sources. Paleoproterozoic amphibolites were impacted by subduction-modified mantle fluids, whereas gabbros most likely evolved from a mantle source modified by subduction slab melts. According to the aforementioned results, there is a back-arc extension in the North China Craton's subduction setting [115,140,141]. Furthermore, a depleted mantle source is

indicated by the extremely positive initial $\varepsilon Nd(t)$ values, particularly in the gabbros. This demonstrates that a subduction environment was used to form the Wutai mafic gabbros.

We concluded that the back-arc extension along the eastern block of the North China Craton's western margin was crucial in altering metasomatic agents related to subduction in the mantle wedge above it, which affected the lithological and geochemical properties of the magmatic rocks. There is compelling evidence that the Wutai Complex was formed in a prolonged subduction tectonic setting due to the discovery of mafic intrusions that date from the Late Archean to the Paleoproterozoic (Figure 18a,b). The region's shift from Archean crust formation to Paleoproterozoic tectonic reworking and stabilization is highlighted by the ages, which show evidence of two separate magmatic pulses.

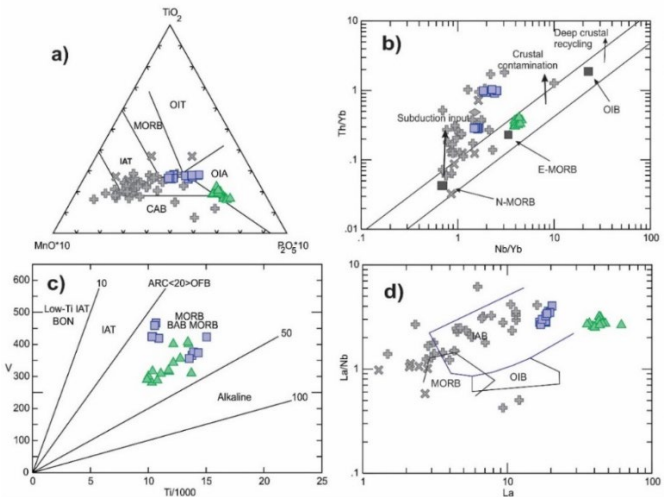

Figure 17. Plots of **(a)** MnO-TiO_2/10-P_2O_5 diagram after (Mullen 1983); **(b)** V *vs.* Ti/1000 diagram after [138]; **(c)** Th/Yb *vs* Nb/Yb diagram after [142]; **(d)** La/Nb *vs.* La diagram after [37].

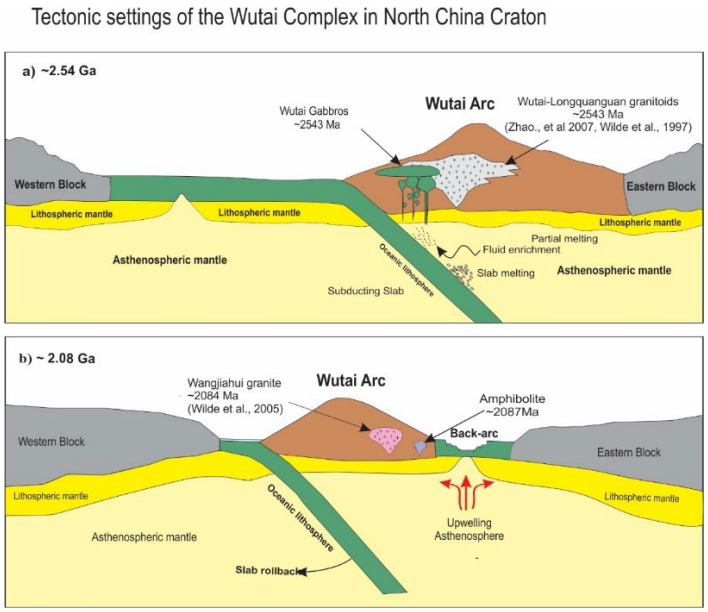

Figure 18. Schematic tectonic evolution model for the Wutai Complex during Late Archean **(a)** Subduction setting (~2543 Ma); shows subduction-related metasomatic agents which influenced the lithological and geochemical transitions in mafic gabbroic intrusion. **(b)** Back arc rift setting (~2087 Ma) during Paleoproterozoic.

8. Conclusion

(1) The ~2.54 Ga gabbros in the Wutai Complex originated from a juvenile, depleted mantle wedge metasomatized by slab-derived melts. These melts were generated through 1%–5% partial melting of a garnet- and spinel-bearing lherzolite mantle source, followed by modification through subduction-related processes.

(2) The ~2.08 Ga amphibolites in the Wutai Complex were generated by ~15% partial melting of garnet-spinel lherzolite and spinel lherzolite mantle sources, which had undergone metasomatism by slab-derived fluids and sediment melts.

(3) The latest Neoarchean and Paleoproterozoic mafic rocks in the Wutai Complex, reflecting an oceanic subduction setting. These results underscore a tectonic transition from Late Archean oceanic subduction to Paleoproterozoic lithospheric extension in the North China Craton, indicating that plate tectonics at least partly happened most likely in the latest Neoarchean.

Acknowledgments

We are grateful to the editor and the three anonymous reviewers for their constructive comments, which have greatly improved the manuscript. This study was supported by the National Natural Science Foundation of China (42425205 and 42402204) and MOST Special Fund from the State Key Laboratory of Continental Dynamics.

Authors' contribution

Zubair Raja Asim: data curation, investigation, formal analysis, writing—original draft, writing—review & editing. Yujing Wang: data curation, investigation, formal analysis, writing—review & editing. Bin Wu: writing—review & editing. Caiyun Lan: writing—review & editing. Xiaoping Long: conceptualization, supervision, project administration, writing-review & editing, funding acquisition, investigation. All authors have read and agreed to the published version of the manuscript.

Conflict of interests

The authors declare no conflict of interest.

References

[1] Zhao G, Wilde SA, Cawood PA, Sun M. Archean blocks and their boundaries in the North China Craton: lithological, geochemical, structural and P–T path constraints and tectonic evolution. *Precambrian Res.* 2001, 107(1–2):45–73.

[2] Zhao G, Cawood PA, Li S, Wilde SA, Sun M, *et al*. Amalgamation of the North China Craton: key issues and discussion. *Precambrian Res.* 2012, 222:55–76.

[3] Liu S, Pan Y, Xie Q, Zhang J, Li Q. Archean geodynamics in the Central Zone, North China Craton: constraints from geochemistry of two contrasting series of granitoids in the Fuping and Wutai complexes. *Precambrian Res.* 2004, 130(1–4):229–249.

[4] Zhao G, Cawood P, Lu L. Petrology and P–T history of the Wutai Amphibolites: implications for tectonic evolution of the Wutai Complex, China. *Precambrian Res.* 1999, 93(2–3):181–199.

[5] Wang K, Li J, Hao J, Li J, Zhou S. The Wutaishan Orogenic Belt within the Shanxi Province, Northern China: a record of Late Archaean collision tectonics. *Precambrian Res.* 1996, 78(1–3): 95–103.

[6] Zhao G, Wilde S, Cawood P, Lu L. Thermal evolution of Archean basement rocks from the eastern part of the North China Craton and its bearing on tectonic setting. *Int. Geol. Rev.* 1998, 40(8):706–721.

[7] Yang Q, Santosh M. The building of an Archean microcontinent: evidence from the North China Craton. *Gondwana Res.* 2017, 50:3–37.

[8] Gao P, Santosh M, Kwon S, Kim SW. Ocean plate stratigraphy of a long-lived Precambrian subduction-accretion system: the Wutai Complex, North China Craton. *Precambrian Res.* 2021, 363:106334.

[9] Wu C, Zhong C. The Paleoproterozoic SW–NE collision model for the Central North China Craton. *Prog. Precambrian Res.* 1998, 21(3):28–50.

[10] Zhao J, Zhou M. Geochemistry of Neoproterozoic mafic intrusions in the Panzhihua district (Sichuan Province, SW China): implications for subduction-related metasomatism in the upper mantle. *Precambrian Res.* 2007, 152(1–2):27–47.

[11] Wilde SA, Zhao G, Sun M. Development of the North China Craton during the Late Archaean and its final amalgamation at 1.8 Ga: some speculations on its position within a global Palaeoproterozoic supercontinent. *Gondwana Res.* 2002, 5(1):85–94.

[12] Kröner A, Wilde S, O'Brien PJ, Li J, Passchier C, *et al*. Field relationships, geochemistry, zircon ages and evolution of a Late Archaean to Palaeoproterozoic lower crustal section in the Hengshan Terrain of Northern China. *Acta Geol. Sin.* 2005, 79(5):605–629.

[13] Kröner A, Wilde S, Li J, Wang K. Age and evolution of a Late Archean to Paleoproterozoic upper to lower crustal section in the Wutaishan/Hengshan/Fuping terrain of Northern China. *J. Asian Earth Sci.* 2005, 24(5):577–595.

[14] Zhang J, Zhao G, Li S, Sun M, Liu S, *et al*. Deformation history of the Hengshan Complex: implications for the tectonic evolution of the Trans-North China Orogen. *J. Struct. Geol.* 2007, 29(6):933–949.

[15] Zhang J, Zhao G, Li S, Sun M, Wilde SA, *et al*. Polyphase deformation of the Fuping Complex, Trans-North China Orogen: structures, SHRIMP U–Pb zircon ages and tectonic implications. *J. Struct. Geol.* 2009, 31(2):177–193.

[16] Kusky TM, Li J, Tucker RD. The Archean Dongwanzi Ophiolite Complex, North China Craton: 2.505-billion-year-old oceanic crust and mantle. *Science* 2001, 292(5519):1142–1145.

[17] Kusky T, Li J, Santosh M. The Paleoproterozoic North Hebei Orogen: North China Craton's collisional suture with the Columbia supercontinent. *Gondwana Res.* 2007, 12(1–2):4–28.

[18] Polat A, Kusky T, Li J, Fryer B, Kerrich R, *et al*. Geochemistry of Neoarchean (ca. 2.55–2.50 Ga) volcanic and ophiolitic rocks in the Wutaishan Greenstone Belt, Central Orogenic Belt, North China Craton: implications for geodynamic setting and continental growth. *Geol. Soc. Am. Bull.* 2005, 117(11–12):1387–1399.

[19] Kusky TM, Li J. Paleoproterozoic tectonic evolution of the North China Craton. *J. Asian Earth Sci.* 2003, 22(4):383–397.

[20] Li J, Kusky T. A Late Archean foreland fold and thrust belt in the North China Craton: implications for early collisional tectonics. *Gondwana Res.* 2007, 12(1–2):47–66.

[21] Faure M, Trap P, Lin W, Monié P, Bruguier O. The formation of the North China Craton by two Palaeoproterozoic continental collisions in Lüliang-Hengshan-Wutaishan-Fuping massifs. *Episodes* 2007, 30(1):1–12.

[22] Trap P, Faure M, Lin W, Monié P. Late Paleoproterozoic (1900–1800 Ma) nappe stacking and polyphase deformation in the Hengshan–Wutaishan area: implications for the understanding of the Trans-North-China Belt, North China Craton. *Precambrian Res.* 2007, 156(1–2):85–106.

[23] Trap P, Faure M, Lin W, Bruguier O, Monié P. Contrasted tectonic styles for the Paleoproterozoic evolution of the North China Craton. Evidence for a ~2.1 Ga thermal and tectonic event in the Fuping Massif. *J. Struct. Geol.* 2008, 30(9):1109–1125.

[24] Trap P, Faure M, Lin W, Monié P, Meffre S, *et al*. The Zanhuang Massif, the second and eastern suture zone of the Paleoproterozoic Trans-North China Orogen. *Precambrian Res.* 2009, 172(1–2):80–98.

[25] Wang Z. Tectonic evolution of the Hengshan–Wutai–Fuping complexes and its implication for the Trans-North China Orogen. *Precambrian Res.* 2009, 170(1–2):73–87.

[26] Li S, Hart S, Wu T. Rb-Sr and Sm-Nd isotopic dating of an early Precambrian spilite-keratophyre sequence in the Wutaishan area, North China: preliminary evidence for Nd-isotopic homogenization in the mafic and felsic lavas during low-grade metamorphism. *Precambrian Res.* 1990, 47(3–4):191–203.

[27] Zhao G, Wilde SA, Cawood PA, Lu L. Thermal evolution of two textural types of mafic granulites in the North China Craton: evidence for both mantle plume and collisional tectonics. *Geol. Mag.* 1999, 136(3):223–240.

[28] Guo JH, O'Brien PJ, Zhai M. High-pressure granulites in the Sanggan area, North China Craton: metamorphic evolution, P–T paths and geotectonic significance. *J. Metamorph. Geol.* 2002, 20(8):741–756.

[29] Zhao G, Wilde SA, Cawood PA, Lu L. Petrology and P–T path of the Fuping mafic granulites: implications for tectonic evolution of the central zone of the North China Craton. *J. Metamorph. Geol.* 2000, 18(4):375–391.

[30] Gao P, Santosh M. Building the Wutai Arc: insights into the Archean–Paleoproterozoic crustal evolution of the North China Craton. *Precambrian Res.* 2019, 333:105429.

[31] Wilde S, Zhao G, Wang K, Sun M. First SHRIMP zircon U-Pb ages for Hutuo Group in Wutaishan: further evidence for Palaeoproterozoic amalgamation of North China Craton. *Chin. Sci. Bull.* 2004, 49:83–90.

[32] Zhao J, Zhou M. Geochemistry of Neoproterozoic mafic intrusions in the Panzhihua district (Sichuan Province, SW China): implications for subduction-related metasomatism in the upper mantle. *Precambrian Res.* 2007, 152(1–2):27–47.

[33] Li J, Wang K, Wang Q, Liu X, Zhao Z. Early Proterozoic Collision Orogenic Belt in Wutaishan area, China. *Chin. J. Geol.* 1990, 25(1):1–11.

[34] Sun D, Li Q, Liu S, Chen X, Wang Z, *et al*. Neoarchean-Paleoproterozoic magmatic arc evolution in the Wutai-Hengshan-Fuping area, North China Craton: new perspectives from zircon U–Pb ages and Hf isotopic data. *Precambrian Res.* 2019, 331:105368.

[35] Bai J. *The early Precambrian geology of Wutaishan*, 1st ed. Tianjin: Tianjin Science and Technology Press, 1986. p. 475.
[36] Wang K, Zhou S, Hao J. The metamorphism and significance of kyanite-bearing assemblages from the original Jingangku formation of Wutaishan area. *Acta Petrol. Sin.* 1996, 12(1):88–98.
[37] Pearce JA, Cann JR. Tectonic setting of basic volcanic rocks determined using trace element analyses. *Earth Planet. Sci. Lett.* 1973, 19(2):290–300.
[38] Pearce JA. Basalt geochemistry used to investigate past tectonic environments on Cyprus. *Tectonophysics* 1975, 25(1–2):41–67.
[39] Pearge J, Flower M. The relative importance of petrogenetic variables in magma genesis at accreting plate margins: a preliminary investigation. *J. Geol. Soc.* 1977, 134(2):103–127.
[40] Wood DA. The application of a ThHfTa diagram to problems of tectonomagmatic classification and to establishing the nature of crustal contamination of basaltic lavas of the British Tertiary Volcanic Province. *Earth Planet. Sci. Lett.* 1980, 50(1):11–30.
[41] Stolz A, Jochum K, Spettel B, Hofmann A. Fluid-and melt-related enrichment in the subarc mantle: evidence from Nb/Ta variations in island-arc basalts. *Geology* 1996, 24(7):587–590.
[42] Münker C. Nb/Ta fractionation in a Cambrian arc/back arc system, New Zealand: source constraints and application of refined ICPMS techniques. *Chem. Geol.* 1998, 144(1–2):23–45.
[43] Rubatto D, Hermann J. Zircon formation during fluid circulation in eclogites (Monviso, Western Alps): implications for Zr and Hf budget in subduction zones. *Geochim. Cosmochim. Acta* 2003, 67(12):2173–2187.
[44] Liu S, Pan Y, Li J, Li Q, Zhang J. Geological and isotopic geochemical constraints on the evolution of the Fuping Complex, North China Craton. *Precambrian Res.* 2002, 117(1–2):41–56.
[45] Wang Z, Wilde SA, Wang K, Yu L. A MORB-arc basalt–adakite association in the 2.5 Ga Wutai Greenstone Belt: Late Archean magmatism and crustal growth in the North China Craton. *Precambrian Res.* 2004, 131(3–4):323–343.
[46] Tatsumi Y, Hamilton D, Nesbitt R. Chemical characteristics of fluid phase released from a subducted lithosphere and origin of arc magmas: evidence from high-pressure experiments and natural rocks. *J. Volcanol. Geotherm. Res.* 1986, 29(1–4):293–309.
[47] Plank T, Langmuir C. Sediments melt and basaltic crust dehydrates at subduction zones. *Eos Trans. AGU* 1992, 73:637.
[48] Peacock SM, Rushmer T, Thompson AB. Partial melting of subducting oceanic crust. *Earth Planet. Sci. Lett.* 1994, 121(1–2):227–244.
[49] Keppler H. Constraints from partitioning experiments on the composition of subduction-zone fluids. *Nature* 1996, 380(6571):237–240.
[50] Hawkesworth CJ, Gallagher K, Hergt J, McDermott F. Trace element fractionation processes in the generation of island arc basalts. *Philos. Trans. R. Soc. Lond. A* 1993, 342(1663):179–191.
[51] Hawkesworth C, Turner S, McDermott F, Peate D, Van Calsteren P. U-Th isotopes in arc magmas: implications for element transfer from the subducted crust. *Science* 1997, 276(5312):551–555.
[52] Elliott R, Baker S, Rogers R, O'leary D, Paykel E, *et al*. Prefrontal dysfunction in depressed patients performing a complex planning task: a study using positron emission tomography. *Psychol. Med.* 1997, 27(4):931–942.

[53] Rollinson HR, Tarney J. Adakites—the key to understanding LILE depletion in granulites. *Lithos* 2005, 79(1–2):61–81.

[54] Wilson M. Mid-ocean ridges. In *Igneous petrogenesis*, 1st ed. Berlin: Springer, 1989. pp. 101–150.

[55] Jin B. *The early Precambrian geology of Wutaishan,* 1st ed. Tianjin: Science and Technology Press, 1986. pp. 7–63,401.

[56] Tian Z, Han P, Xu K. The Mesozoic-Cenozoic East China rift system. *Tectonophysics* 1992, 208(1–3):341–363.

[57] Bai J, Wang R, Guo J. The major geologic events of Early Precambrian and their dating in Wutaishan region. *Beijing, Geological Publishing House* 1992:34–55.

[58] Jahn B, Auvray B, Shen Q, Liu D, Zhang Z, *et al*. Archean crustal evolution in China: the Taishan Complex, and evidence for juvenile crustal addition from long-term depleted mantle. *Precambrian Res.* 1988, 38(4):381–403.

[59] Jahn BM, Gruau G, Capdevila R, Cornichet J, Nemchin A, *et al*. Archean crustal evolution of the Aldan Shield, Siberia: geochemical and isotopic constraints. *Precambrian Res.* 1998, 91(3–4):333–363.

[60] Jahn B, Zhang Z. Archean granulite gneisses from eastern Hebei Province, China: rare earth geochemistry and tectonic implications. *Contrib. Mineral. Petrol.* 1984, 85:224–243.

[61] Condie KC. Episodic continental growth and supercontinents: a mantle avalanche connection? *Earth Planet. Sci. Lett.* 1998, 163(1–4):97–108.

[62] Dusel-Bacon C, Cooper KM. Trace-element geochemistry of metabasaltic rocks from the Yukon-Tanana Upland and implications for the origin of tectonic assemblages in east-central Alaska. *Can. J. Earth Sci.* 2000, 36(10):1671–1695.

[63] Puchtel IS, Hofmann AW, Amelin YV, Garbe-Schönberg CD, Samsonov A, *et al*. Combined mantle plume-island arc model for the formation of the 2.9 Ga Sumozero-Kenozero Greenstone Belt, SE Baltic Shield: isotope and trace element constraints. *Geochim. Cosmochim. Acta* 1999, 63(21):3579–3595.

[64] Baksi AK. Search for a deep-mantle component in mafic lavas using a Nb Y Zr plot. *Can. J. Earth Sci.* 2001, 38(5):813–824.

[65] Deniel C. Geochemical and isotopic (Sr, Nd, Pb) evidence for plume–lithosphere interactions in the genesis of Grande Comore magmas (Indian Ocean). *Chem. Geol.* 1998, 144(3–4):281–303.

[66] Fitton J, Saunders A, Norry M, Hardarson B, Taylor R. Thermal and chemical structure of the Iceland plume. *Earth Planet. Sci. Lett.* 1997, 153(3–4):197–208.

[67] Zhang Z, Wu J, Xe X. Rb-Sr and Sm-Nd ages of the Archean metamorphic rocks of the lower Fuping subgroup and their implications. *Geochimica* 1991, 2:118–126.

[68] Jin B, Ruzheng W, Jinjing G. *The major geological events of early Precambrian and their age dating in the Wutai Region,* 1st ed. Beijing: Geological Publishing House. 1992.

[69] Sun M, Armstrong RL, Lambert RSJ. Petrochemistry and Sr, Pb, and Nd isotopic geochemistry of early Precambrian rocks, Wutaishan and Taihangshan areas, China. *Precambrian Res.* 1992, 56(1–2):1–31.

[70] Yongjun L, Shuwen L, Zhao G, Qiugen L, Zhang J, *et al*. Geochemistry and petrogenesis of Neoarchean metamorphic mafic rocks in the Wutai Complex. *Acta Geol. Sin.* 2006, 80(6):899–911.

[71] Tian Y. *Geology and mineralization of the Wutai-Hengshan Greenstone Belt*, 1st ed. Taiyuan: Shanxi Science and Technology Press, 1991. pp. 137–152.

[72] Wilde S, Cawood P, Wang K, Nemchin A. The relationship and timing of granitoid evolution with respect to felsic volcanism in the Wutai Complex, North China Craton. In *Proceedings of the 30th IGC. Precambrian Geology and Metamorphic Petrology*, Beijing, China, August 4–14, 1996, pp. 75–88.

[73] Wilde SA, Zhao G. Archean to Paleoproterozoic evolution of the North China Craton. *J. Asian Earth Sci.* 2005, 24(5):519–522.

[74] Wu Y, Zheng Y. Genesis of zircon and its constraints on interpretation of U-Pb age. *Chin. Sci. Bull.* 2004, 49:1554–1569.

[75] Grimes CB, John BE, Kelemen P, Mazdab F, Wooden J, *et al*. Trace element chemistry of zircons from oceanic crust: a method for distinguishing detrital zircon provenance. *Geology* 2007, 35(7):643–646.

[76] Polat A, Kerrich R. Archean Greenstone Belt magmatism and the continental growth–mantle evolution connection: constraints from Th–U–Nb–LREE systematics of the 2.7 Ga Wawa subprovince, Superior Province, Canada. *Earth Planet. Sci. Lett.* 2000, 175(1–2):41–54.

[77] Le Bas M. A chemical classification of volcanic rocks based on the total alkali-silica system. *J. Petrol.* 1986, 27:247–257.

[78] Winchester JA, Floyd PA. Geochemical discrimination of different magma series and their differentiation products using immobile elements. *Chem. Geol.* 1977, 20:325–343.

[79] Sun S, McDonough W. Chemical and isotopic systematics of oceanic basalts: implications for mantle composition and processes. In *Magmatism in the Ocean Basins*, 1st ed. London: Geological Society of London, 1989. pp. 313–345.

[80] Weaver BL. The origin of ocean island basalt end-member compositions: trace element and isotopic constraints. *Earth Planet. Sci. Lett.* 1991, 104(2–4):381–397.

[81] DePaolo DJ. Trace element and isotopic effects of combined wallrock assimilation and fractional crystallization. *Earth Planet. Sci. Lett.* 1981, 53(2):189–202.

[82] Pearce J, Peate D. Tectonic implications of the composition of volcanic ARC magmas. *Annu. Rev. Earth Planet. Sci.* 1995, 23(1):251–285.

[83] Wilson M, Downes H, Woodhead J, Eggins S, Gamble J. High field strength and transition element systematics in island arc and back-arc basin basalts: evidence for multi-phase melt extraction and a depleted mantle wedge. *Earth Planet. Sci. Lett.* 1993, 114:491–504.

[84] Elliott T, Plank T, Zindler A, White W, Bourdon B. Element transport from slab to volcanic front at the Mariana arc. *J. Geophys. Res.: Solid Earth* 1997, 102(B7):14991–15019.

[85] Hart SR, Dunn T. Experimental cpx/melt partitioning of 24 trace elements. *Contrib. Mineral. Petrol.* 1993, 113(1):1–8.

[86] Johnson KT. Experimental determination of partition coefficients for rare earth and high-field-strength elements between clinopyroxene, garnet, and basaltic melt at high pressures. *Contrib. Mineral. Petrol.* 1998, 133(1):60–68.

[87] Plank T. Nb and Ta in arc and mid-ocean ridge basalts. In *AGU Fall Meeting (American Geophysical Union Fall Meeting),* San Francisco, USA, December 4–8, 1995, p. F655.

[88] Woodhead J, Eggins S, Gamble J. High field strength and transition element systematics in island arc and back-arc basin basalts: evidence for multi-phase melt extraction and a depleted mantle wedge. *Earth Planet. Sci. Lett.* 1993, 114(4):491–504.

[89] Kepezhinskas P, McDermott F, Defant MJ, Hochstaedter A, Drummond MS, *et al*. Trace element and Sr–Nd–Pb isotopic constraints on a three-component model of Kamchatka Arc petrogenesis. *Geochim. Cosmochim. Acta* 1997, 61(3):577–600.

[90] Wedepohl KH. The composition of the continental crust. *Geochim. Cosmochim. Acta* 1995, 59(7):1217–1232.

[91] Aldanmaz E, Pearce JA, Thirlwall M, Mitchell J. Petrogenetic evolution of Late Cenozoic, post-collision volcanism in Western Anatolia, Turkey. *J. Volcanol. Geotherm. Res.* 2000, 102(1–2):67–95.

[92] Green NL. Influence of slab thermal structure on basalt source regions and melting conditions: REE and HFSE constraints from the Garibaldi Volcanic Belt, Northern Cascadia subduction system. *Lithos* 2006, 87(1–2):23–49.

[93] Johnson K. Experimental cpx/and garnet/melt partitioning of REE and other trace elements at high pressures: petrogenetic implications. *Mineral. Mag.* 1994, 58:454–455.

[94] McKenzie D, O'nions R. Partial melt distributions from inversion of rare earth element concentrations. *J. Petrol.* 1991, 32(5):1021–1091.

[95] Defant M, Jackson T, Drummond Md, De Boer J, Bellon H, *et al*. The geochemistry of young volcanism throughout Western Panama and Southeastern Costa Rica: an overview. *J. Geol. Soc.* 1992, 149(4):569–579.

[96] Hastie PA, de Ojeda DM, Luquin AC. A review of research on sport education: 2004 to the present. *Phys. Educ. Sport Pedagog.* 2011, 16(2):103–132.

[97] Castillo PR. Adakite petrogenesis. *Lithos* 2012, 134:304–316.

[98] Gazel E, Hoernle K, Carr MJ, Herzberg C, Saginor I, *et al*. Plume–subduction interaction in southern Central America: mantle upwelling and slab melting. *Lithos* 2011, 121(1–4):117–134.

[99] Straub KM, Paola C, Kim W, Sheets B. Experimental investigation of sediment-dominated *vs.* tectonics-dominated sediment transport systems in subsiding basins. *J. Sediment. Res.* 2013, 83(12):1162–1180.

[100] Imaoka T, Nakashima K, Kamei A, Itaya T, Ohira T, *et al*. Episodic magmatism at 105 Ma in the Kinki district, SW Japan: petrogenesis of Nb-rich lamprophyres and adakites, and geodynamic implications. *Lithos* 2014, 184:105–131.

[101] Sun SS, McDonough W. Chemical and isotopic systematics of oceanic basalts: implications for mantle composition and processes. In *Magmatism in the Ocean Basins*, 1st ed. London: Geological Society of London, 1989. pp. 313–345.

[102] Polat A, Kerrich R. Geodynamic processes, continental growth, and mantle evolution recorded in Late Archean Greenstone Belts of the southern Superior Province, Canada. *Precambrian Res.* 2001, 112(1–2):5–25.

[103] Pearce JA, Stern RJ. Origin of back-arc basin magmas: trace element and isotope perspectives. In *Back-arc spreading systems: Geological, biological, chemical, and physical interactions,* Washington: American Geophysical Union (AGU), 2006, pp. 63–86.

[104] Pearce JA, Stern RJ, Bloomer SH, Fryer P. Geochemical mapping of the Mariana arc-basin system: implications for the nature and distribution of subduction components. *Geochem. Geophys. Geosyst.* 2005, 6(7).

[105] Elliott T. Tracers of the slab. In *Geophysical Monograph-American Geophysical Union*, 1st ed. Washington: American Geophysical Union (AGU), 2003. pp. 23–46.

[106] McCulloch MT, Gamble J. Geochemical and geodynamical constraints on subduction zone magmatism. *Earth Planet. Sci. Lett.* 1991, 102(3–4):358–374.

[107] Manning CE. The chemistry of subduction-zone fluids. *Earth Planet. Sci. Lett.* 2004, 223(1–2):1–16.

[108] Jenner FE, O'Neill HSC. Analysis of 60 elements in 616 ocean floor basaltic glasses. *Geochem. Geophys. Geosyst.* 2012, 13(2).

[109] Gribble RF, Stern RJ, Bloomer SH, Stüben D, O'Hearn T, *et al*. MORB mantle and subduction components interact to generate basalts in the southern Mariana Trough back-arc basin. *Geochim. Cosmochim. Acta* 1996, 60(12):2153–2166.

[110] Gribble RF, Stern RJ, Newman S, Bloomer SH, O'Hearn T. Chemical and isotopic composition of lavas from the northern Mariana Trough: implications for magmagenesis in back-arc basins. *J. Petrol.* 1998, 39(1):125–154.

[111] Stolper E, Newman S. The role of water in the petrogenesis of Mariana Trough magmas. *Earth Planet. Sci. Lett.* 1994, 121(3–4):293–325.

[112] Grove T, Parman S, Bowring S, Price R, Baker M. The role of an H 2 O-rich fluid component in the generation of primitive basaltic andesites and andesites from the Mt. Shasta region, N California. *Contrib. Mineral. Petrol.* 2002, 142:375–396.

[113] Kogiso T, Tatsumi Y, Nakano S. Trace element transport during dehydration processes in the subducted oceanic crust: 1. experiments and implications for the origin of ocean island basalts. *Earth Planet. Sci. Lett.* 1997, 148(1–2):193–205.

[114] Green TH. Significance of Nb/Ta as an indicator of geochemical processes in the crust-mantle system. *Chem. Geol.* 1995, 120(3–4):347–359.

[115] Kepezhinskas P, Defant MJ, Drummond MS. Progressive enrichment of island arc mantle by melt-peridotite interaction inferred from Kamchatka xenoliths. *Geochim. Cosmochim. Acta* 1996, 60(7):1217–1229.

[116] Peng P, Zhai M, Zhang H, Guo J. Geochronological constraints on the Paleoproterozoic evolution of the North China Craton: SHRIMP zircon ages of different types of mafic dikes. *Int. Geol. Rev.*2005, 47(5):492–508.

[117] Guan H, Sun M, Wilde SA, Zhou X, Zhai M. SHRIMP U–Pb zircon geochronology of the Fuping Complex: implications for formation and assembly of the North China Craton. *Precambrian Res.* 2002, 113(1–2):1–18.

[118] Zhao G, Wilde SA, Cawood PA, Sun M. SHRIMP U–Pb zircon ages of the Fuping Complex: implications for Late Archean to Paleoproterozoic accretion and assembly of the North China Craton. *Am. J. Sci.* 2002, 302(3):191–226.

[119] Liu D, Page R, Compston W, Wu J. U-Pb zircon geochronology of Late Archaean metamorphic rocks in the Taihangshan—Wutaishan area, North China. *Precambrian Res.* 1985, 27(1–3):85–109.

[120] Xia X, Sun M, Zhao G, Fuyuan W, Ping X, *et al*. U-Pb Age and Hf isotope study of detrital zircons from the Wanzi Supracrustals: constraints on the tectonic setting and evolution of the Fuping Complex, Trans-North China Orogen. *Acta Geol. Sin. (Engl. Ed.)* 2006, 80(6):844–863.

[121] Tang L, Santosh M. Neoarchean-Paleoproterozoic terrane assembly and Wilson cycle in the North China Craton: an overview from the central segment of the Trans-North China Orogen. *Earth Sci. Rev.* 2018, 182:1–27.

[122] Wilde SA, Cawood PA, Wang K, Nemchin AA. Granitoid evolution in the Late Archean Wutai Complex, North China Craton. *J. Asian Earth Sci.* 2005, 24(5):597–613.

[123] Du L, Yang C, Wang W, Ren L, Wan Y, *et al*. Paleoproterozoic rifting of the North China Craton: geochemical and zircon Hf isotopic evidence from the 2137 Ma Huangjinshan A-type granite porphyry in the Wutai area. *J. Asian Earth Sci.* 2013, 72:190–202.

[124] Shi Y, Yu J, Santosh M. Tectonic evolution of the Qinling Orogenic Belt, Central China: new evidence from geochemical, zircon U–Pb geochronology and Hf isotopes. *Precambrian Res.* 2013, 231:19–60.

[125] Tang L, Santosh M. Neoarchean Granite-Greenstone Belts and related ore mineralization in the North China Craton: an overview. *Geosci. Front.* 2018, 9(3):751–768.

[126] Sengör AC, Natal'In BA. Turkic-type orogeny and its role in the making of the continental crust. *Annu. Rev. Earth Planet. Sci.* 1996, 24(1):263–337.

[127] Polat A, Kerrich R, Wyman D. The Late Archean Schreiber–Hemlo and White River–Dayohessarah Greenstone Belts, Superior Province: collages of oceanic plateaus, oceanic arcs, and subduction–accretion complexes. *Tectonophysics* 1998, 289(4):295–326.

[128] Wan Y, Song B, Liu D, Wilde SA, Wu J, *et al*. SHRIMP U–Pb zircon geochronology of Palaeoproterozoic metasedimentary rocks in the North China Craton: evidence for a major Late Palaeoproterozoic tectonothermal event. *Precambrian Res.* 2006, 149(3–4):249–271.

[129] Liu D, Nutman A, Compston W, Wu J, Shen Q. Remnants of ≥ 3800 Ma crust in the Chinese part of the Sino-Korean Craton. *Geology* 1992, 20(4):339–342.

[130] Nutman A, Chadwick B, Krishna Rao B, Vasudev V. SHRIMP U/Pb zircon ages of acid volcanic rocks in the Chitradurga and Sandur groups, and granites adjacent to the Sandur Schist Belt, Karnataka. *J. Geol. Soc. India* 1996, 47(2):153–164.

[131] Zhao H, Seibert SE, Hills GE. The mediating role of self-efficacy in the development of entrepreneurial intentions. *J. Appl. Psychol.* 2005, 90(6):1265.

[132] Defant MJ, Drummond MS. Derivation of some modern arc magmas by melting of young subducted lithosphere. *Nature* 1990, 347(6294):662–665.

[133] Drummond M, Defant M, Kepezhinskas P. Petrogenesis of slab-derived trondhjemite–tonalite–dacite/adakite magmas. *Earth Environ. Sci. Trans. R. Soc. Edinburgh* 1996, 87(1–2):205–215.

[134] Hawkins JW. Geology of supra-subduction zones-implications for the origin of ophiolites. In *Ophiolite Concept and the Evolution of Geological Thought*, 1st ed. Boulder: Geological Society of America (GSA), 2003. pp. 227–240.

[135] Tatsumi Y. High-Mg andesites in the Setouchi Volcanic Belt, Southwestern Japan: analogy to Archean magmatism and continental crust formation? *Annu. Rev. Earth. Planet. Sci.* 2006, 34(1):467–499.

[136] Hanyu T, Tatsumi Y, Nakai Si, Chang Q, Miyazaki T, *et al*. Contribution of slab melting and slab dehydration to magmatism in the NE Japan Arc for the last 25 Myr: constraints from geochemistry. *Geochem. Geophys. Geosyst.* 2006, 7(8).

[137] Mullen ED. MnO/TiO2/P2O5: a minor element discriminant for basaltic rocks of oceanic environments and its implications for petrogenesis. *Earth Planet. Sci. Lett.* 1983, 62(1):53–62.

[138] Shervais JW. Ti-V plots and the petrogenesis of modern and ophiolitic lavas. *Earth Planet. Sci. Lett.* 1982, 59(1):101–118.

[139] Shinjo R, Chung SL, Kato Y, Kimura M. Geochemical and Sr-Nd isotopic characteristics of volcanic rocks from the Okinawa Trough and Ryukyu Arc: implications for the evolution of a young, intracontinental back arc basin. *J. Geophys. Res.: Solid Earth* 1999, 104(B5):10591–10608.

[140] Sajona FG, Maury RC, Bellon H, Cotten J, Defant MJ, *et al*. Initiation of subduction and the generation of slab melts in Western and Eastern Mindanao, Philippines. *Geology* 1993, 21(11):1007–1010.

[141] Hastie AR, Mitchell SF, Kerr AC, Minifie MJ, Millar IL. Geochemistry of rare high-Nb basalt lavas: are they derived from a mantle wedge metasomatised by slab melts? *Geochim. Cosmochim. Acta* 2011, 75(17):5049–5072.

[142] Pearce JA. Geochemical fingerprinting of oceanic basalts with applications to ophiolite classification and the search for Archean oceanic crust. *Lithos* 2008, 100(1–4):14–48.